

**Study of salinity retrieval errors
for the SMOS mission**

Carolina Gabarró Prats

Doctoral thesis

Advisors: Dr. Jordi Font Ferré and Dr. Adriano Camps Carmona

Dept. de Geologia Marina i Oceanografia Física.
Institut de Ciències del Mar (CSIC), Barcelona

November 2004

A la meva família i especialment a la meva
tieta àvia, que des del primer moment
em va animar a realitzar aquesta tesi.

Agraïments

Ja de petita deia que volia investigar, sense saber massa què significava, però la idea d'explorar allò desconegut em fascinava (de fet, encara em passa ara). També volia ser astronauta, volia veure l'immens espai des de més a prop, i la Terra des de lluny. Bé, no sóc ni una cosa ni l'altra però em sento propera a les dues.

Vull agrair a totes les persones que m'han ajudat en aquest llarg camí que representa fer una tesi.

En primer lloc dono les gràcies als meus directors, el Jordi i l'Adriano, pel seu inestimable ajut i per animar-me a acabar aquesta tesi, en moments que tenia dubtes de si continuar-la o deixar-la. D'ells he après moltíssim.

També agraeixo als meus pares i al meu germà el suport incondicional i la confiança que m'han mostrat durant tot aquest temps i sempre. I vull fer especial menció de la tieta Mari, la meva tieta àvia, que té 93 anys i que des del primer moment em va encoratjar a fer la tesi: em deia que era una molt bona cosa, que m'obriria camins en el futur i que o bé la feia ara, o ja no la faria mai. Tant de bo jo pugui tenir la ment tan clara com ella a la seva edat. Gràcies tieta.

Evidentment, també vull agrair al Marc tot el que ha fet per ajudar-me en els moments de nervis, d'estrès i d'esgotament que m'han acompanyat aquests últims mesos. Gràcies per la comprensió i per fer-me riure quan més ho necessitava.

També, dono les gràcies a l'Agustí per tot el que m'ha ensenyat, a tots els companys del grup d'oceanografia física, amb qui he après, rigut i compartit tantes coses, així com a la Mercè i altra gent del TSC amb qui he pogut comptar sempre que he tingut dubtes.

Vull agrair als meus companys de despatx, el Jordi S., el Jordi I. i l'Antonio el seu incansable ajut, sobretot per resoldre problemes del Latex. També a la Maribel, a la Teresa i a la Sílvia pel seu suport moral i a la resta dels comensals de la taula rodona pels dinars compartits. També a altres persones de l'Institut que m'han ajudat al llarg d'aquest temps.

Vull fer aparèixer en aquests agraïments els amics amb qui he compartit diferents etapes de la meva vida i que m'han fet costat també en aquesta. A tots ells els estimo i necessito: l'Olga, el Marc, el Lluís, l'Anna, la Sònia, la Bea, la Tat, el Miquel, l'Àdam, la Nata, el Ferri, la Cristina, el Miquel, la Glòria, la Marissa, el Pere, la Sílvia, la Marta, la Circe, l' Alicia, el Fer, el Dani, la Mònica, el Lluís, el Martin, l'Oriol, la Mireia, el Joan Carles, la Marta, l'Ingrid, i encara més gent però la llista comença ja a ser massa llarga.

Bé, en definitiva, a totes aquelles persones que m'han envoltat, ajudat, estimat i cuidat en tot aquest temps. Gràcies a tots.

Resum

El treball realitzat en aquesta tesi està emmarcat en la missió SMOS (Soil Moisture and Ocean Salinity) de l'Agència Espacial Europea. El satèl·lit es llançarà el febrer del 2007, i mesurarà la salinitat superficial del mar i la humitat del sòl. L'instrument (MIRAS) consisteix en un radiòmetre interferomètric en banda L (1,400-1,430 GHz). Serà la primera vegada que es posarà en òrbita un instrument d'aquestes característiques i que es mesuraran aquests paràmetres des de l'espai. No obstant, encara son molts els aspectes científics que queden per resoldre. Aquesta tesi, doncs, ha intentat abordar alguns del temes oberts en la recuperació de la salinitat a partir de les mesures de SMOS.

La sensibilitat de la temperatura de brillantor (el què el radiòmetre mesura) a la salinitat és màxima, tot i que no és gaire gran, a la freqüència de 1,4 GHz. Per altra banda la sensibilitat a la temperatura superficial del mar i a la rugositat és del mateix ordre de magnitud. Això implica que per recuperar la salinitat amb una certa precisió, cal també conèixer aquests altres paràmetres anomenats auxiliars.

La recerca feta en aquesta tesi està gairebé tota basada en dades experimentals de diferents campanyes que s'han realitzat utilitzant diferents radiòmetres en banda L, més boies i altres instruments per mesurar les variables in situ.

S'ha fet un estudi sobre diferents models d'emissivitat en banda L de la superfície del mar, que existeixen en l'actualitat. Aquests models, tant teòrics com semi-empírics, s'han utilitzat per recuperar, de la temperatura de brillantor mesurada, la salinitat. Aquesta salinitat recuperada s'ha comparat amb les dades de salinitat adquirides in situ. Els resultats han demostrat que els models semi-empírics recuperen millor la salinitat que no pas els teòrics que s'han analitzat en aquest treball.

Els models actuals descriuen la rugositat del mar en funció únicament del vent present. En alguns casos això no és correcte (mar de fons, mars no totalment desenvolupats). Així, analitzant aquestes limitacions, l'autora proposa un nou model semi-empíric, derivat de dades de la campanya WISE. Aquest model descriu la temperatura de brillantor deguda a la rugositat del mar amb dos paràmetres: la velocitat del vent i l'alçada significativa de l'ona. Aquest nou model resulta ser el que recupera salinitat amb més qualitat a partir de dades radiomètriques de tres campanyes diferents, que s'han realitzat amb diferents instruments i en diverses condicions del mar.

Errors en els paràmetres auxiliars, especialment en la velocitat del vent, degraden la qualitat de la salinitat recuperada. En aquesta tesi, diferents fonts d'informació vent i onatge s'han utilitzat per recuperar la salinitat: models meteorològics i oceanogràfics i dades de satèl·lit. Utilitzant com a paràmetres auxiliars dades obtingudes de models, la salinitat es recupera amb millor qualitat (probablement perquè aquests tenen més resolució espacial i temporal que no pas les mesures des de satèl·lit). De totes maneres aquesta conclusió no es pot extrapol·lar, ja que això només s'ha provat en una zona geogràfica (la Mediterrània occidental).

En aquesta tesi es proposa obtenir aquests paràmetres auxiliars de les mateixes mesures radiomètriques, així com es fa amb la salinitat. Degut a la configuració de SMOS, cada píxel serà vist des de diferents angles d'incidència. Això ens permetrà poder recuperar més d'una variable, ja que estem tractant un sistema sobredeterminat. El mètode d'inversió és, aleshores, capaç de recuperar salinitat, velocitat del vent, onatge i la temperatura superficial del mar. Ara bé, quan utilitzem mètodes d'inversió amb restriccions s'obtenen millors resultats. Això consisteix en donar al sistema un valor de referència i el seu error per cada paràmetre. Amb aquest mètode l'error en la salinitat recuperada és de l'ordre de 0.2 psu, mentre que el vent recuperat té un error aproximat de 1 m/s, precisió que no és possible obtenir amb cap model ni satèl·lit simultani al pas de SMOS.

Per acabar, s'ha recuperat la salinitat d'imatges de temperatura de brillantor generades amb el simulador de SMOS. Aquestes imatges tenen la configuració de SMOS i estan afectades d'errors instrumentals, sorolls i biaixos, tal com passarà en el sensor real. Els resultats ens demostren que calen encara molts esforços per buscar una manera de reduir tots aquests errors i així augmentar la qualitat de la salinitat recuperada.

Abstract

This PhD thesis has been done in the framework of the SMOS (Soil Moisture and Ocean Salinity) mission, from the European Space Agency. This satellite will be launched in February 2007 and will provide global sea surface salinity and soil moisture maps, variables that never have been measured before from space. The payload instrument (MIRAS) is an L-band interferometric radiometer. This will be the first time an instrument with this characteristics is put in orbit. However, there are still a lot of issues that need to be solved. This thesis is focused on some open questions of the salinity retrieval process from SMOS measurements.

The sensitivity of the brightness temperature to salinity is maximum at the frequency of 1.4 GHz, even though this sensitivity is not high. The brightness temperature at this frequency is also sensitive to sea surface temperature and to sea surface roughness. Therefore to retrieve salinity with good quality it is necessary to know those parameters, as well.

An important part of the thesis work is based on experimental data obtained from different campaigns, which have been performed mainly in preparation of SMOS. During the campaigns different L-band radiometers have been used as well as buoys and other instruments to measure the in situ parameters.

A study of different sea surface emissivity models has been performed. Several theoretical and semi-empirical models have been used to retrieve salinity from measured brightness temperatures. The retrieved salinity has been compared with the measured, one and results have shown that the semi-empirical models retrieve better salinity than the analysed theoretical models.

Most of the emissivity models consider the roughness as function of the local wind speed, only. In the cases where swell or not fully developed seas are present this is not a good assumption. Therefore, the author proposes a new semi-empirical model derived from the WISE campaign. This new model describes the brightness temperature due to the roughness with two parameters: wind speed and significant wave height. When this model is used, the salinity is retrieved from radiometric data with better quality for three different campaigns data sets performed with different radiometers and in different sea conditions.

Errors on the auxiliary parameters produce additional not negligible errors on the retrieved salinity. Different sources of wind speed and wave height have been used to retrieve salinity: meteorological and oceanographic models and satellite measurements. Better results on the retrieved salinity are obtained, when model

output data are used. This is probably due to their higher spatial and temporal resolution. However, this conclusion can not be extrapolated, since it has been analysed only in one geographical area (Western Mediterranean).

The author proposes then to obtain the auxiliary parameters from the radiometric measurements themselves, as well as salinity. Due to the SMOS configuration, each pixel is seen from different incidence angles. This configures then an overdetermined system, and more than one variable can be retrieved. Therefore the inversion method is capable to retrieve salinity, wind speed, wave height and sea surface temperature. However, better results are obtained when some restrictions are used in the inversion; it is to give reference values and its errors for the different variables to the system. Using this method, salinity can be retrieved with an accuracy of 0.2 psu, and wind speed with an accuracy of 1 m/s, a value that is impossible to obtain from models or satellite measurements simultaneous to SMOS.

Finally, salinity has been retrieved from images crated by the SMOS simulator. These images have the real SMOS configuration and suffer from noise, bias and instrumental errors, as will happen to the real sensor. Results show that important efforts should be done to decrease these errors to improve the quality of the retrieved salinity.

Contents

| | | |
|----------|--|-----------|
| 1 | General Introduction | 15 |
| 1.1 | Why do we measure salinity ? | 16 |
| 1.2 | How to measure salinity? | 17 |
| 1.3 | Microwave radiometry: Fundamental concepts | 19 |
| 1.3.1 | Physical principles | 20 |
| 1.3.2 | Brightness temperature sensitivity to geophysical parameters | 25 |
| 1.3.3 | The Stokes parameters | 28 |
| 1.3.4 | Influencing effects on antenna temperature | 29 |
| 1.4 | Microwave radiometer design | 31 |
| 1.4.1 | Real aperture radiometers | 31 |
| 1.4.2 | Synthetic aperture radiometers | 33 |
| 1.5 | Previous salinity missions and campaigns | 34 |
| 1.5.1 | Fixed-based platforms | 34 |
| 1.5.2 | Airborne | 35 |
| 1.5.3 | Spaceborne | 38 |
| 1.6 | Current satellite salinity missions | 38 |
| 1.6.1 | SMOS | 38 |
| 1.6.2 | AQUARIUS | 42 |
| 1.7 | Objectives and thesis plan | 44 |
| 2 | Campaigns | 49 |
| 2.1 | Campaigns with active participation of the author | 50 |
| 2.1.1 | WISE | 50 |
| 2.1.2 | EuroSTARRS | 68 |
| 2.2 | Other campaigns | 70 |
| 2.2.1 | FROG 2003 | 70 |
| 2.2.2 | The Plata Campaign | 71 |

CONTENTS

| | | |
|----------|--|------------|
| 3 | Modelling the brightness temperature of the sea | 77 |
| 3.1 | Theoretical models | 78 |
| 3.1.1 | Dielectric constant models | 78 |
| 3.1.2 | Wave spectrum theoretical models | 81 |
| 3.1.3 | Surface roughness scattering models | 82 |
| 3.2 | Semi-empirical models for sea surface emissivity | 85 |
| 3.2.1 | Wind speed dependence | 85 |
| 3.2.2 | Wave height dependence | 87 |
| 3.2.3 | Wind speed and wave height dependence | 87 |
| 3.3 | Conclusions | 91 |
| 4 | Auxiliary Parameters | 93 |
| 4.1 | Sensitivity to auxiliary parameters | 94 |
| 4.2 | Roughness parameter | 96 |
| 4.3 | SST parameter | 100 |
| 4.4 | Other potential auxiliary parameters | 100 |
| 5 | Salinity Retrieval | 103 |
| 5.1 | Inversion algorithms | 104 |
| 5.1.1 | Cost function | 106 |
| 5.1.2 | Methodology | 107 |
| 5.2 | Number of incidence angles | 107 |
| 5.3 | Models comparison with salinity retrieval | 108 |
| 5.3.1 | Dielectric permittivity models | 108 |
| 5.3.2 | Scattering and wave spectrum models | 110 |
| 5.4 | Impact on retrieved salinity of auxiliary parameters errors | 118 |
| 5.4.1 | Auxiliary parameters obtained from the T_B | 120 |
| 5.5 | Retrieved salinity from the Plata survey | 129 |
| 5.6 | Conclusions | 133 |
| 6 | Salinity retrieved from images generated by the SMOS End-to-End performance simulator | 137 |
| 6.1 | Introduction to SEPS | 138 |
| 6.2 | Retrieval process | 140 |
| 6.3 | Conclusions | 149 |
| 7 | Conclusions and recommendations | 151 |
| 7.1 | Conclusions on emissivity models | 151 |
| 7.2 | Conclusions on auxiliary parameters | 152 |
| 7.3 | Recommendations | 153 |

CONTENTS

| | | |
|----------|---|------------|
| A | Compilation of articles | 155 |
| A.1 | List of articles in which the author has participated | 155 |
| A.2 | International Journal of Remote Sensing | 159 |
| A.3 | Geophysical Research Letters | 177 |
| B | Instrumentation technical documentation | 183 |
| | Bibliography | 187 |

CONTENTS

Chapter 1

General Introduction

This chapter presents a short description of the physical principles of salinity measurements. It reviews the basics of microwave radiometry, and presents, shortly, the types of radiometers existing nowadays. It summarises previous campaigns that intended to measure salinity by radiometry since 1971. And finally two space missions currently under development to measure salinity are presented.

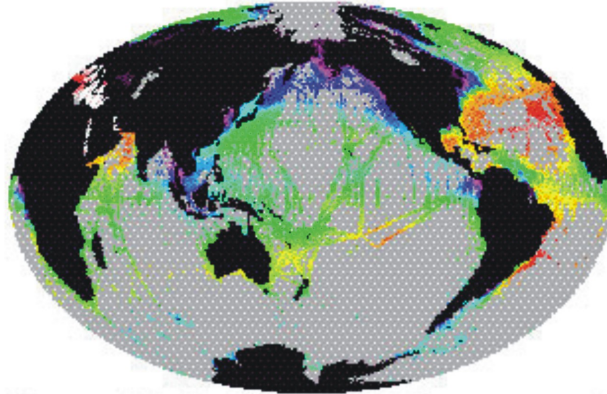


Figure 1.1: 100 years of Sea Surface Salinity measurements. Colours are salinity values. From Aquarius web page (<http://aquarius.gsfc.nasa.gov/overview.html>).

1.1 Why do we measure salinity ?

Human activities seem to have a significant influence on the climate of our planet and public awareness of possible climate changes has increased in the past few years. The scientific community thus faces a challenging task to answer the most pressing questions:

Is the climate actually changing and, if yes, at which rate, and more importantly, what will be the consequences, in particular with respect to the frequency of occurrence of extreme events?

Significant progress has been made in terms of weather forecasting, climate monitoring, and extreme events forecasting during recent years, using sophisticated models fed, among other things, by data acquired with operational satellites and analysed using super-computers. However, as recently pointed out by several working groups further improvement now depends on the availability of global observations of two crucial variables: Soil Moisture (SM) and Sea Surface Salinity (SSS). To date this information is lacking because *in situ* measurements are far from global, and so far no dedicated, long term, SM and SSS space mission has been attempted.

Knowledge of the global distribution of salt in the ocean and of its annual and inter-annual variability, is crucial in helping to understand the role of the ocean in the climate system. Ocean circulation is mainly driven by the momentum and heat fluxes through the atmosphere-ocean interface, which can be partly traced by observation of SSS. In addition, salinity also determines ocean density and

1.2 How to measure salinity?

hence thermohaline circulation. In some regions (e.g. the Arctic), salinity is the most important variable as it controls processes such as deep water formation by determining, jointly with the temperature the water density. This process is a key component in the ocean thermohaline circulation conveyor belt. Ocean salinity is also linked to the oceanic carbon cycle, as it plays a part in establishing the chemical equilibrium which in turn regulates the CO_2 uptake and release. Therefore, the assimilation of SSS into global ocean biogeochemical models could improve estimates of absorption of CO_2 by the oceans.

Monitoring SSS could also be used to improve ENSO (El Niño Southern Oscillation) prediction by numerical models. Present models assimilate temperature and/or altimeter- derived sea level data only. The lack of salinity measurements results in major discrepancies between modelled near-surface and observed currents.

SSS is also correlated with estimates of the net evaporation minus precipitation (E-P) balance. E-P is difficult to measure accurately over the ocean, so global maps of SSS would provide a constraint on estimates of E-P at a global scale.

In situ salinity measurements are only sparsely distributed over the oceans. Examining available data in $1^\circ \times 1^\circ$ boxes over the global oceans shows that salinity measurements exist for only about 70% of them. An even smaller fraction of the boxes contains more than one measurement. As for other oceanographic variables, global monitoring by *in situ* measurements are extremely expensive and a logistically complicated issue. Fig 1.1 shows the measurements of SSS done in 100 years all over the world.

Thereafter, satellite remote sensing, as presently achieved for sea surface temperature (SST) and sea surface height, appears to be an efficient solution to solve the lack of salinity information.

1.2 How to measure salinity?

Salinity is the measure of all the salts dissolved in water and it has traditionally been expressed in parts per thousand (ppt). The average ocean salinity is 35 ppt and the average river water salinity is 0.5 ppt or less. It is that in every kilogram of seawater, 35 grams are salt. Deep water almost always contains more salt than surface waters, since the density of the salty waters is higher.

The salt in the ocean is mostly made up of the elements sodium (Na) and chlorine (Cl). Together they account for 85.7% of the dissolved salt. The other major components of seawater are magnesium (Mg), calcium (Ca), potassium (K) and sulfate (SO_4). Together with chlorine and sodium they make up 99.4% of the salt in the ocean.

1 General Introduction

Originally, salinity was measured by evaporating the water, and the remaining salts weighted. However such method gave unreliable results. Later, it was done by chemical determinations.

Salinity is now determined by measuring how well electricity travels through water, this is also called conductivity. Water that has dissolved salt in it will conduct electricity better than water with no dissolved salt. The more salt dissolved in the water, the better water conducts electricity.

UNESCO (1978) and other international organisations recommended to define salinity using only conductivity, and they defined the *The Practical Salinity Scale* which is now the official definition.

The salinity of a sample of seawater is measured in terms of a ratio, R_T , which is defined as:

$$R_T = C(S, 15, 1)/C(KCl, 15, 1), \quad (1.1)$$

where $C(S, 15, 1)$ is the conductivity of the sea-water sample at temperature 15°C and standard atmospheric pressure (1 atm), and $C(KCl, 15, 1)$ is the conductivity of the standard potassium chloride (KCl) solution, with a concentration of 32.4356g kg^{-1} , at temperature 15°C and standard atmospheric pressure. Then the salinity is related to the conductivity ratio by the following equation:

$$S_{psu} = 0.0080 - 0.1692R_{15}^{1/2} + 25.3851R_{15} + 14.0941R_{15}^{3/2} - 7.0261R_{15}^2 + 2.7081R_{15}^{5/2}. \quad (1.2)$$

Salinity is then a unit-less quantity written as psu for *practical salinity unit*.

Conductivity, that depends on salinity and temperature, is measured by placing platinum electrodes in seawater and measuring the current that flows when there is a known voltage between the electrodes. The current depends on the conductivity, voltage, and volume of sea water in the path between electrodes. If the electrodes are in a tube of non-conducting glass, the volume of water is accurately known, and the current is independent of other objects near the conductivity cell. The best measurements of salinity from conductivity give salinity with an accuracy of $\pm 0.002\text{psu}$.

Nowadays, the most reliable instruments to measure salinity, are the laboratory salinometers which measure conductivity by relative measurements standardised by comparison with 'standard seawater', or also called 'Copenhagen Water'. This standard seawater is produced by diluting a large sample of seawater until it has a precise salinity of 35 psu. A widely-used instrument of this class is the Guildline 8410 Portable Salinometer.

1.3 Microwave radiometry: Fundamental concepts

Microwave radiometry allows us to measure the emissivity of a medium (in this case of sea surface), and Fresnel's equation relates it with the dielectric constant (or permittivity) of sea water. This parameter is dependent on the temperature and also on the type of salt, and its concentration. So, in principle, it is possible to obtain the salinity concentration through that measurement.

After several studies, it has been shown that the sensitivity of brightness temperature to salinity is maximum at low microwave, as shown in figure 1.2, even though it is not very high. The L-band (1.4 GHz-1.43 GHz) is the optimum band for sensing salinity, since it is the first protected one.

At present, two satellite missions are in preparation to measure salinity using L-band radiometry. The present work is mainly a contribution to SMOS (Soil Moisture Ocean Salinity), a European Space Agency mission, planned for launched in 2007. One of its goals is the measurement of sea surface salinity over the oceans with an expected accuracy of 0.1 psu.

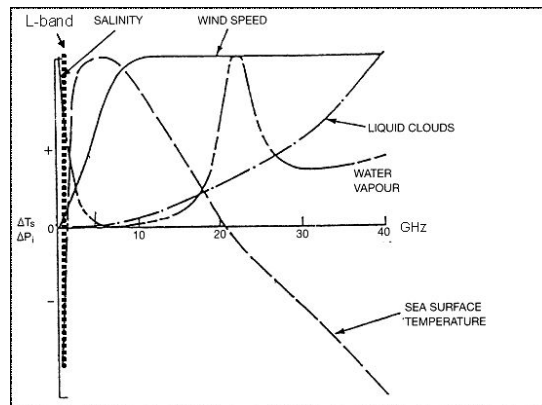


Figure 1.2: Sensitivity of several parameters to frequency.

1.3 Microwave radiometry: Fundamental concepts

The bulk of energy received by the planet Earth is in the form of solar electromagnetic radiation. Part of the incident solar energy is scattered and absorbed by Earth's atmosphere, and the remainder is transmitted to Earth's surface. A part of the latter is scattered outwards and the remainder is absorbed. According to thermodynamic principles, absorption of electromagnetic energy by a material medium leads to a transformation into thermal energy, which is accompanied by a rise in the thermometric temperature of the material. The reverse process, that of 'thermal' emission, serves to create the balance between the absorbed solar

1 General Introduction

radiation and the radiation emitted by the Earth's surface and its atmosphere. These transformation processes are treated by the radiative transfer theory.

Radiometry is the field of science and engineering related to the measurement of radiant electromagnetic energy. All material media (gases, liquids, solids and plasma) radiate (emit) electromagnetic energy, which extends over the entire electromagnetic spectrum. A radiometer is a high sensitive and precise receiver capable of measuring low levels of radiation.

1.3.1 Physical principles

Thermal emission in the microwave region

A blackbody is an idealised body, perfectly opaque material that absorbs all the incident radiation at all frequencies, reflecting none. It is, also, a perfect emitter, since otherwise the energy absorbed by a material would increase its temperature indefinitely. The unpolarised blackbody radiation is emitted according to Planck's radiation law uniformly with a spectral brightness shown in equation 1.3.

$$B_f = \frac{2hf^3}{c^2} \left(\frac{1}{e^{hf/kT} - 1} \right), \quad (1.3)$$

where B_f = Blackbody spectral brightness, $Wm^{-2}sr^{-1}Hz^{-1}$
 h = Planck's constant= $6.63 \times 10^{-34} J s$
 f = frequency, Hz
 k = Boltzmann's constant= $1.38 \times 10^{-23} JK^{-1}$
 T = absolute temperature, K
 c = velocity of light= $3 \times 10^8 ms^{-1}$

In the microwave region, generally $hf \ll kT$ and then the Rayleigh-Jeans approximation can be applied to equation 1.3 as follows.

$$e^x - 1 = \left(1 + x + \frac{x^2}{2} + \dots \right) - 1 \simeq x, \quad \text{for } x \ll 1 \quad (1.4)$$

then,

$$B_f = \frac{2f^2kT}{c^2} = \frac{2kT}{\lambda^2}. \quad (1.5)$$

And then, the brightness of a blackbody B_{bb} at a temperature T , and for a bandwidth of Δf , is:

1.3 Microwave radiometry: Fundamental concepts

$$B_{bb} = B_f \Delta f = \frac{2kT}{\lambda^2} \Delta f. \quad (1.6)$$

Real materials, usually referred as *grey bodies*, do not necessarily absorb all the energy incident upon them, and so emit less than a blackbody does. Then, considering a semi-infinite material, if its brightness, which may be direction-dependent, is $B(\theta, \phi)$ and its physical temperature is T , a blackbody equivalent radiometric temperature may be defined so that $B(\theta, \phi)$ can assume a form similar to 1.6. Such a temperature usually is called the *brightness temperature*, $T_B(\theta, \phi)$, and accordingly,

$$B(\theta, \phi) = \frac{2k}{\lambda^2} T_B(\theta, \phi) \Delta f \quad (1.7)$$

The brightness of a material relative to that of a blackbody at the same temperature is defined as the *emissivity* $e(\theta, \phi)$:

$$e(\theta, \phi) = \frac{B(\theta, \phi)}{B_{bb}} = \frac{T_B(\theta, \phi)}{T} \quad (1.8)$$

Since $B(\theta, \phi) \leq B_{bb}$, $0 \leq e(\theta, \phi) \leq 1$. Thus, the emissivity is a dimensionless quantity ranging from unity (for perfect blackbody) to zero (for perfect reflectors), and it is polarisation dependent. Then, the brightness temperature of a material is always smaller than or equal to its physical temperature. For a flat surface, the emissivity can be written, also, as follows:

$$e(\theta) = 1 - R(\theta), \quad (1.9)$$

where R is the Fresnel power reflection coefficient dependent on the polarisation (horizontal and vertical).

Sea-surface emissivity

It is the surface emissivity at L-Band which carries information regarding SSS. The emissivity and the power reflection coefficient R are related as expressed in 1.9. For a plane surface, R is the Fresnel reflection coefficient, and is dependent on the incident radiation zenith angle θ , and on the complex dielectric constant of sea water, ε :

$$\begin{aligned} R_H &= \left| \frac{\cos \theta - \sqrt{\varepsilon - \sin^2 \theta}}{\cos \theta + \sqrt{\varepsilon - \sin^2 \theta}} \right|^2, \\ R_V &= \left| \frac{\varepsilon \cos \theta - \sqrt{\varepsilon - \sin^2 \theta}}{\varepsilon \cos \theta + \sqrt{\varepsilon - \sin^2 \theta}} \right|^2. \end{aligned} \quad (1.10)$$

1 General Introduction

Figure 1.3 illustrates the general shape of the variation of emissivity as function on the incidence angle.

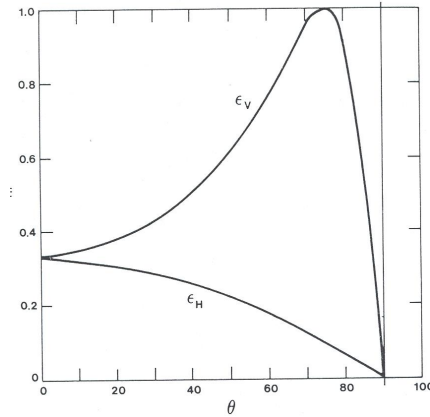


Figure 1.3: Typical shape of the horizontal and vertical emissivity with the incidence angle (from Swift (1980)).

The complex dielectric constant (or permittivity) of the sea water is dependent on temperature and on the concentration of salt. It can be calculated at any frequency, within the microwave band, from Debye (1929) expression:

$$\varepsilon = \varepsilon_{\infty} + \frac{(\varepsilon_s - \varepsilon_{\infty})}{1 + i\omega\tau} - i\frac{\sigma}{\omega\varepsilon_0}, \quad (1.11)$$

in which i is the imaginary number, ε_{∞} is the electrical permittivity at very high frequencies, ε_s is the static dielectric constant, τ is the relaxation time, σ is the ionic conductivity, and $\varepsilon_0 = 8.854 * 10^{-12} F/m$ is the permittivity of free space. ε_s, τ and σ are functions of the temperature and salinity of sea-water, and have been evaluated by Klein and Swift (1977), Ellison et al. (1998) and Blanch and Aguiasca (2004) (these models will be explained later in this document).

Skin depth of sea surface emission

In a conducting medium, a high frequency signal will only penetrate a limited depth into the material. The penetration depth will depend on the frequency of the radiation and on the conductivity of the medium. Thus on the sea, the penetration depth depends on the salinity as well as the frequency. The skin depth δ_s is defined as the distance into the medium at which the power of the electromagnetic radiation is reduced by a factor e^{-2} .

1.3 Microwave radiometry: Fundamental concepts

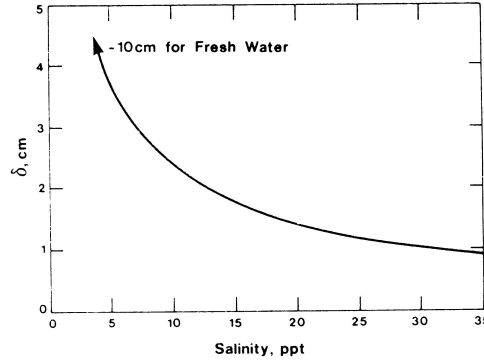


Figure 1.4: Variation of electromagnetic penetration depth with sea-water salinity, at 1.43 GHz and 20° C (from Swift (1980)).

Figure 1.4 shows that as the salinity is reduced the skin depth increases, up to about 10 cm for fresh water. So, for open oceans (approx. 35 psu), the penetration depth at L-band is less than 1 cm, at 20° C.

Radiation received by the antenna

The microwave radiometric measurement is the brightness temperature, which is defined in equation 1.8, as $T_B(\theta, \phi) = \epsilon(\theta, \phi)T$ and its sensitivity is proportional to $(B\tau)^{-1/2}$, where B is the bandwidth and τ is the integration time. Hence, for precision radiometry it is desirable to use a bandwidth as large as possible, because for a radiometer on a moving platform the upper limit on τ usually is constrained by the platform parameters (height and speed) as well as antenna beamwidth and scanning configuration.

The *apparent temperature* $T_{AP}(\theta, \phi)$ is the energy incident to the antenna in the direction of the main lobe. The most influent term to T_{AP} is the brightness temperature of the pixel, T_B , at which the antenna is pointing. However other sources are also measured by the antenna; one is the atmospheric self-emission, denoted by T_{UP} . Another source sensed by the antenna is the radiometric temperature scattered by the terrain (T_{SC}) in the direction (θ, ϕ) , formed by the addition of two terms: the reflected downward emitted atmospheric radiation (T_{DN}) and the reflected extraterrestrial radiation. The terms emitted by the sea ($T_B + T_{SC}$) are attenuated by the atmospheric loss factor L_a as the energy travels from the terrain to the antenna (see figure 1.5). So,

$$T_{AP} = T_{UP} + (T_B + T_{SC}) \frac{1}{L_a}, \quad (1.12)$$

1 General Introduction

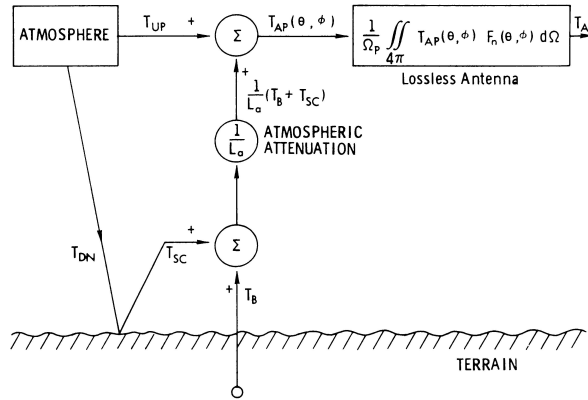
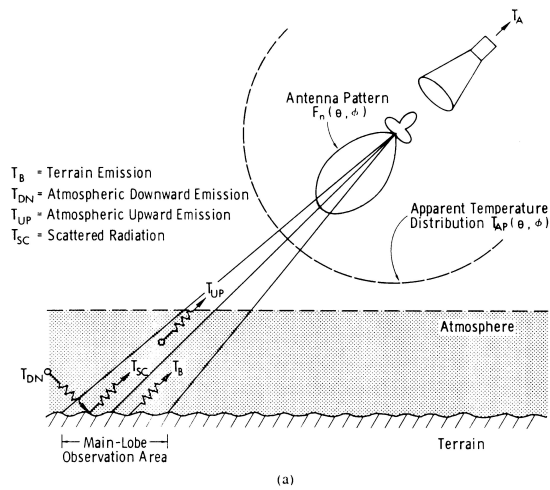


Figure 1.5: a) Schematic representation of the relationship between T_B , T_A and T_{AP} , b) block-diagram representation (from Ulaby et al. (1981)).

1.3 Microwave radiometry: Fundamental concepts

and

$$T_A = \frac{A_r}{\lambda} \iint_{4\pi} T_{AP}(\theta, \phi) F_n(\theta, \phi) d\Omega. \quad (1.13)$$

The antenna temperature, T_A , is the integral of the apparent temperature multiplied by the antenna pattern (see equation 1.13), therefore side and back lobes of the antenna pick up energy from other areas that are not the target. The aim of antenna design is to achieve a power pattern having a strong narrow main beam and low side lobes, so that T_A is a good approximation of the average value of T_B .

The power measured by an antenna observing a thermally radiating background can be related to an *antenna temperature*, by using the Rayleigh-Jeans approximation as follows:

$$P = kBGT_A \quad (1.14)$$

where B is the bandwidth of the system and G the gain of the radiometer.

One characteristic of radiometric measurements is that at microwave frequencies the emission is very weak, and the signal received at the sensor is therefore weak, even in some cases, smaller than the receiver's noise power. Also, for this reason, it is necessary to work under frequency bands protected, at least theoretically, against human emissions of any kind, otherwise they would mask the signal to be measured.

Frequently passive microwave systems share frequency allocations with radio astronomy, this is the case of the range of 1.400-1.427 GHz at L-band. Additional frequencies have been allocated for radiometry on a shared basis, but some points of the globe will be inaccessible for their sensing due to radio frequency interference (RFI).

1.3.2 Brightness temperature sensitivity to geophysical parameters

Figure 1.6 shows that sensitivity of the dielectric constant to the salinity is maximum at low microwave frequencies, so the best conditions for sensing salinity from space are found at low microwave frequencies and at protected bands. So, the range from 1.4-1.427 GHz, which holds at L-band, is established for sensing salinity.

However it must be stressed that, even being the best situation, sensitivity of the brightness temperature to the SSS at this frequency, is low: 0.5 K/psu for a sea surface temperature of 20°C, decreasing to 0.25 K/psu for a SST of 0° C,

1 General Introduction

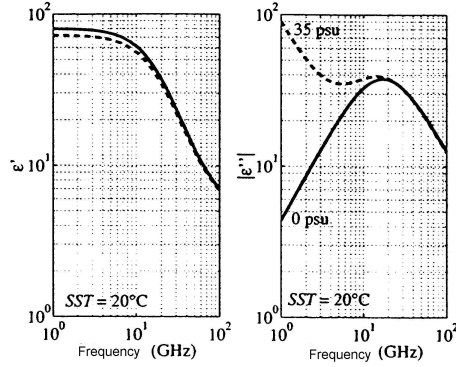


Figure 1.6: Sea water dielectric constant for 35 psu and for pure water, as function of frequency, computed with Klein and Swift (1977) model. On the left, real part of ϵ , on the right the imaginary part of ϵ (from Dinnat (2003)).

both at nadir (Skou, 1995, Lagerloef et al., 1995, Lagerloef, 1998). Figure 1.7 shows the sensitivity of T_B to salinity as a function of the incidence angle, and it indicates that the vertical polarisation is about 30% more sensitive to the SSS than the horizontal polarisation.

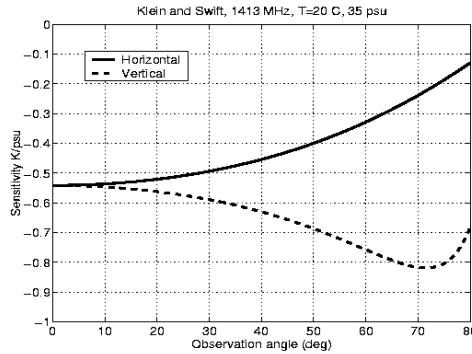


Figure 1.7: Sensitivity to sea surface salinity at L-band.

Figure 1.8 illustrates the resulting variation of brightness temperature for different SST and salinity conditions at L-Band. It shows that the brightness temperature is more sensitive to SSS for warm and more saline waters and that at high salinities the brightness temperature actually decreases as SST increases.

Since other variables than SSS influence the T_B signal (sea surface temper-

1.3 Microwave radiometry: Fundamental concepts

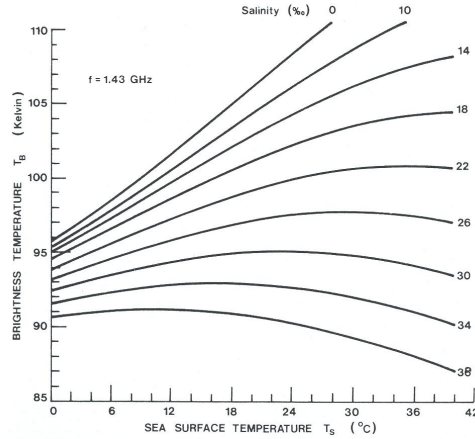


Figure 1.8: Variation of brightness temperature at normal incidence with SST, for different water salinities, at 1.43 GHz (from Swift (1980)).

ature, surface roughness and foam), the accuracy of the SSS measurement will degrade unless these other influencing effects are properly accounted for.

The sensitivity of T_B to sea surface temperature is not slight, and it depends on the salinity concentration and on the incidence angle, the maximum is $0.6 K/^\circ C$. However, near 35 psu and $25^\circ C$ it is near to zero.

Experimental data-sets reveal a sensitivity to wind speed extrapolated at nadir of $\sim 0.23K/(m/s)$, or somewhat higher $\sim 0.25K/(m/s)$ when the atmospheric instability or only the measurements corresponding to $U_{10} > 2 m/s$ are accounted for (Camps et al., 2004a). This sensitivity increases at H-polarisation up to $\sim 0.5K/(m/s)$ at 65° , and decreases at V-polarisation down to $\sim -0.2K/(m/s)$ at 65° , with a zero-crossing around $55^\circ-60^\circ$. From this information one realises that the effect on T_B of an increment of wind speed of 1m/s, is approximately similar to a change of 1 psu of sea surface salinity.

A modulation of the instantaneous brightness temperatures due to wave slopes (and also foam) has been observed, and makes the standard deviation of this modulation increase with wind speed at a rate of $\sim 0.1 - 0.15K/(m/s)$, depending on polarisation, and very weakly on incidence angle. Sensitivity of T_B with respect to significant wave height is about $\sim 1K/m$, extrapolated at nadir, increasing at H-polarisation up to $\sim 1.5K/m$ at 65° , and decreasing at V-polarisation down to $\sim -0.5K/m$ at 65° .

In addition, a small azimuthal modulation $\sim 0.2 - 0.3K$ peak to peak has been observed for low-to-moderate wind speeds. However, very large peak-to-peak modulations of 4-5 K have been also observed during a strong storm, which

1 General Introduction

cannot be predicted with current numerical methods and sea surface spectra. A full analysis of these results is presented in Camps et al. (2004a).

Campaigns data confirm a small, but non-negligible impact of the presence of sea foam on the L-band brightness temperature at wind speeds above 10 m/s. The foam effect could represent an increment on the T_B of about $\sim 0.2 - 0.3$ K for typical values of 1-2% of foam coverage at $U_{10} \approx 15$ m/s (Villarino et al., 2003).

1.3.3 The Stokes parameters

Any plane wave can be decomposed in two orthogonally polarised components, horizontal and vertical polarisations, as follows:

$$E(z, t) = E_h(z, t)\vec{h} + E_v(z, t)\vec{v}, \quad (1.15)$$

and each projection is defined as:

$$\begin{aligned} E_h(t) &= \text{Re}\{E_{0h}(t)e^{-j\omega t}\} = E_{0h}(t) \cos(\omega t + \delta_h), \\ E_v(t) &= \text{Re}\{E_{0v}(t)e^{-j\omega t}\} = E_{0v}(t) \cos(\omega t + \delta_v), \end{aligned} \quad (1.16)$$

where E_{0h} and E_{0v} are the amplitudes of the \vec{E} field, at H-polarisation and V-polarisation respectively, ω is the instantaneous wave frequency and δ_h and δ_v are the phase factors ($\delta = \delta_v - \delta_h$).

The four Stokes parameters are a very useful way to describe the polarisation state of an electromagnetic wave, even if it is a full polarised, partial or non-polarised wave. The Stokes parameters describe the total energy transported by the wave and the kind of polarisation. Then the Stokes parameters can be defined as:

$$\begin{bmatrix} I \\ Q \\ U \\ V \end{bmatrix} = \begin{bmatrix} T_H + T_V \\ T_V - T_H \\ T_{45^\circ} - T_{-45^\circ} \\ T_{l\text{ cir}} - T_{r\text{ cir}} \end{bmatrix} = \frac{\lambda^2}{kB\eta} \begin{bmatrix} \langle |E_h|^2 \rangle + \langle |E_v|^2 \rangle \\ \langle |E_h|^2 \rangle - \langle |E_v|^2 \rangle \\ 2\text{Re}\langle E_v E_h^* \rangle \\ 2\text{Im}\langle E_v E_h^* \rangle \end{bmatrix} \quad (1.17)$$

where λ is the radiometer's wavelength, k is Boltzmann constant, B the bandwidth and η is the medium impedance (air).

I represents the total power transported by the wave, Q is the difference between the power brought by the H-pol and the V-pol, and represent the linear polarisation oriented in the reference direction. U represents the linear polarisation component oriented in $+45^\circ$ and -45° . V is interpreted as the difference between left-hand and right-hand circularly polarised brightness temperature.

1.3 Microwave radiometry: Fundamental concepts

Both U and V can be measured by two total power radiometers or by a complex correlation radiometer.

If the wave is completely coherent then, $I = Q^2 + U^2 + V^2$, if not, this results in an inequality, $I^2 > Q^2 + U^2 + V^2$. If the wave is completely unpolarised then $Q=U=V=0$.

Polarimetric radiometers measure the energy coming at H-pol and V-pol separately and they usually use what is called the modified Stokes vector. Expressing energies in terms of brightness temperatures, it results:

$$\vec{T}_B = \begin{bmatrix} T_H \\ T_V \\ T_3 \\ T_4 \end{bmatrix} = \frac{\lambda^2}{kB\eta} \begin{bmatrix} \langle |E_h|^2 \rangle \\ \langle |E_v|^2 \rangle \\ 2Re\langle E_v E_h^* \rangle \\ 2Im\langle E_v E_h^* \rangle \end{bmatrix}. \quad (1.18)$$

Then, it can be defined $T_1 = T_h + T_v$ and $T_2 = T_v - T_h$, that are the equivalent of the first and second Stokes parameters.

1.3.4 Influencing effects on antenna temperature

Several effects external from the instrument can induce errors on the brightness temperature measurements. Yueh et al. (2001) made an exhaustive study of the possible error sources which could effect the accuracy of the salinity retrieved from microwave radiometric measurements. Some of the most important problems are reviewed hereafter.

Faraday rotation

The plane of polarisation of microwave radiation that travels from Earth's surface through the ionosphere to the satellite is rotated by an angle φ (Faraday rotation). The amount of rotation depends on the position of the ray path with respect to the Earth's geomagnetic field and on the ionospheric electron content.

This rotation is higher for low microwave frequencies, and as SMOS measurements require a great accuracy, this factor should be taken in consideration. An average daytime rotation angle can be calculated as:

$$\varphi = 17^\circ / f^2, \quad (1.19)$$

where f is in GHz, so at L-band the mean rotation angle is 8.7° during daytime, but depending on the hours and the incidence angle, this value can reach 28° (Skou (2003)).

As SMOS will have a 6 a.m. orbit, the Faraday rotation will be between 5° and 10° . Then it will mix the polarisations as follows:

1 General Introduction

$$\begin{aligned} T_{Bh}^F &= T_{Bh} \cos^2(\varphi) + T_{Bv} \sin^2(\varphi), \\ T_{Bv}^F &= T_{Bh} \sin^2(\varphi) + T_{Bv} \cos^2(\varphi). \end{aligned} \quad (1.20)$$

This could produce errors on the brightness temperature of the order of 2 K, which results in errors on the retrieved salinity between 2 and 4 psu.

If the first Stokes parameter is used, as shown in equation 1.17, I is the sum of vertical and horizontal polarisations, such as: $I = T_{Bh}^F + T_{Bv}^F = T_{Bh}(\cos^2(\varphi) + \sin^2(\varphi)) + T_{Bv}(\sin^2(\varphi) + \cos^2(\varphi)) = T_{Bh} + T_{Bv}$, thereby measurements are independent of Faraday rotation.

However, the problem when using this method is that less independent measurements are obtained, half of them, which can lead to less accuracy in the retrieved SSS. This aspect is nowadays under study.

Atmospheric and extraterrestrial sources

As explained briefly in section 1.3.1, atmospheric attenuation and emission affect over-ocean brightness temperature measured at 1.4 GHz.

Equation 1.12 express the apparent temperature observed by the satellite radiometer viewing the earth and considering the atmospheric consequences. Atmospheric effects at 1.4 GH are determined primarily by rain, clouds, water vapour and atmospheric oxygen content (Goodberlet and Miller, 1997).

$T_{UP}(h)$ is the brightness temperature of upwelling atmosphere emission as seen by a downward looking radiometer at altitude (h in km), and it can be approximated by (Ulaby et al., 1981):

$$T_{UP}(h) \approx (0.412h - 0.030h^2)/\cos(\theta). \quad (1.21)$$

$T_{SC}(\theta, p)$, which is polarisation dependent, is the brightness temperature scattered by sea surface. It is due to two factors:

$$\begin{aligned} T_{SC}(f, \theta, p) &= R(f, \theta, p)(T_{DN}(f, \theta, p) + T_{EXT}(\theta)) \\ &= [1 - e(f, \theta, p)](T_{DN}(f, \theta, p) + T_{EXT}(\theta)), \end{aligned} \quad (1.22)$$

where T_{DN} , is the downwelling atmospheric emission as seen by an upward looking radiometer at the ocean surface. The calculation of this parameter is described in Ulaby et al. (1981) and at 1.4 GHz it can be approximated to $2.1/\cos(\theta)$ in K.

T_{EXT} is the brightness temperature of extraterrestrial sources, which consists of two terms : $T_{EXT} = T_{COS} + T_{GAL}$.

1.4 Microwave radiometer design

T_{COS} is referred to as the cosmic background temperature, and it is a remnant of the origin of the universe in a 'Big Bang'. At 1.4 GHz it is essentially constant in both space and time with a value of 2.7 K.

T_{GAL} represents the average emission of our galaxy, the Milky Way. At frequencies above 5 GHz it can be neglected, but at 1.4 GHz until now it was approximated to 1.3 K. However, a recent study by Le Vine and Abraham (2004), shows that at L-band the galactic brightness temperature can be important and that unlike the cosmic background, this radiation is spatially and temporal variable and it is polarised. These authors present a radiometric map of the sky at L-band, and T_{GAL} can vary (over a perfectly reflecting surface) between 1 - 6 K depending on the orientation of the sensor and orbit, and the season. The highest values are observed near the galactic plane. This is an important issue that needs to be deeper analysed for SMOS.

1.4 Microwave radiometer design

The type of instrument that is used to measure the radiation from real materials is normally referred to as a radiometer, or in this case a microwave radiometer. In this part of the spectrum, the Rayleigh-Jeans approximation is valid, thus the power received by the radiometer is $P = kBGT_A$, where G is the gain of the radiometer and B is the bandwidth of the system.

1.4.1 Real aperture radiometers

The received power is extremely small, so the receiver must be very sensitive. Furthermore, in real life, the noise produced by the radiometer itself (T_N) is added to the input signal. Because the brightness temperature signal is also a noise signal (since it is incoherent radiation) and both signals are independent, they will add and cannot be separated later.

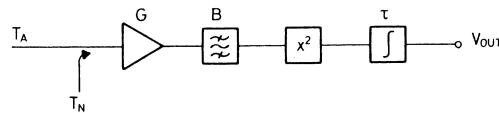


Figure 1.9: Total power radiometer diagram representation (from Skou (1989)).

For the case of a *total power radiometer* (see figure 1.9), $V_{out} = c(T_A + T_N)G$

1 General Introduction

is totally dependent on T_N and G , and in general, this is not stable enough to satisfy reasonable requirements of absolute accuracy.

The basic radiometer design in remote sensing applications is the *Dicke radiometer*. The principle of this radiometer is not to measure directly the antenna temperature, but rather the difference between this and a known reference value, called T_R (see figure 1.10). Then the sensitivity of the measurement to gain and noise temperature instabilities is greatly reduced. The input of the radiometer rapidly ($F_s = 1000Hz$) switches between antenna temperature and a reference load which is known.

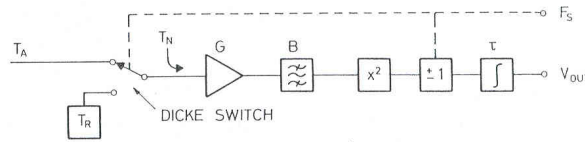


Figure 1.10: Dicke radiometer diagram representation (from Skou (1989)).

Then the output of the radiometer is given by the following expression:

$$V_{out} = c(T_A - T_R)G \quad (1.23)$$

Here T_N is eliminated, but G is still present, while with less weight, since T_R is in the same range as T_A . This configuration gives less sensitivity to instabilities, but poorer sensitivity is achieved, since half of the measurement time is spent on the antenna signal. The sensitivity is degraded by a factor of 2 as compared with the total power radiometer.

The *noise-injection radiometer* (NIR) represents another step forward for better accuracy, since the output is independent of gain and noise temperature. This radiometer is a specialisation of a Dicke radiometer in which the output is always zero, controlled by a servo loop.

Figure 1.11 shows that this configuration uses a Dicke radiometer, with the difference that the input signal to the Dicke radiometer is $T'_A = T_A + T_I$, where T_I is the output of a variable noise generator, and that T'_A (the input to the Dicke radiometer) has the same value as the reference temperature T_R , and a zero output results. A servo-loop adjusts T_I to maintain the zero output condition. So the output value is independent to the gain, as follows:

$$V_{out} = c(T'_A - T_R)G = 0 \quad (1.24)$$

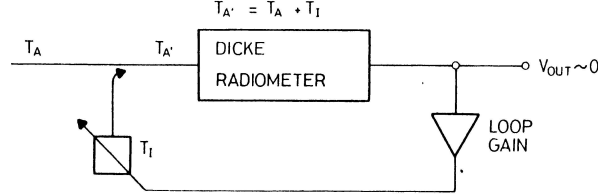


Figure 1.11: Noise-Injection radiometer diagram representation (from Skou (1989)).

$$T_A = T_R - T_I \quad (1.25)$$

The sensitivity of the noise-injection radiometer is found using:

$$\Delta T = 2 \frac{T_R + T_N}{\sqrt{B\tau}} \quad (1.26)$$

More information can be found in Ulaby et al. (1981).

1.4.2 Synthetic aperture radiometers

When dealing with real aperture radiometers, the angular resolution can be described in a rough approximation (since it depends on antenna design and on gain) as $\beta = \lambda/D$ radians, where D is the diameter of the antenna. Thus the required antenna size for a given footprint d is $D = \lambda h/d$. Therefore, at L-band ($\lambda = 21$ cm), a radiometer flying at 700 km would need an antenna of 5 m in diameter to have a 30 km footprint, thus an antenna of such dimensions is complicated to put in orbit.

By using interferometric radiometers, this problem is solved. This technique uses many small receivers, that measure the phase difference of the incident radiation. By cross-correlating the radiofrequency (RF) signals received by each pair of antennas that have an overlapping FOV, a two-dimensional image is created. In this way a big antenna is "synthesised" simulated, and a high angular resolution is achieved.

Real aperture radiometers image the brightness temperature by scanning their antenna across the field of view (FOV). The resolution of the image is consequently determined by the beamwidth of the antenna. Interferometric imaging radiometers, on the other hand, generate an image indirectly by measuring the Fourier transform of the brightness temperature distributed over the FOV.

1 General Introduction

This measurement is referred as the visibility function and is, afterwards, inverse Fourier transformed to form the image.

SMOS will be the first satellite that will carry a 2-D synthetic aperture radiometer at L-band. Only the synthetic aperture technique allows a reasonable spatial resolution measurement.

For more information about 2-D synthetic aperture technique refer to Camps (1996) and Ruf (1988).

1.5 Previous salinity missions and campaigns

During nearly 40 years, several campaigns and studies have been carried out to investigate the possibility of measuring sea surface salinity from radiometric acquisitions. Here we make a short presentation of some of these scientific studies, split into three different kinds of platforms used.

1.5.1 Fixed-based platforms

A fixed ocean platform provides the advantages of high spatial resolution on sea surface, excellent ground truth, and a relative ease of radiometer calibration and determination of antenna characteristics as compared to an aircraft platform. In addition, there is not a need for correcting atmospheric losses between the antenna and the sea.

Argus Island Tower measurements - Hollinger

The measurements described by Hollinger (1971) were made from Argus Island tower at 1.41, 8.36 and 19.34 GHz, in March 1970. Argus Island is located approximately 45 km south-west of Bermuda at 60 m of water depth. The microwave radiometers consisted of a parabolic antenna and linearly polarised feed system followed by a conventional Dicke receiver. Since the antennas were able to rotate around their electrical axes, any plane of linear polarisation could be measured, so the vertical and horizontal components were acquired. Measurements were made at a series of incremented incidence angles (5-10 degrees). The absolute error in antenna temperature and the relative errors in the brightness temperature were about $\pm 2K$. The absolute errors on the brightness temperature were about 5 to 10 percent.

The conclusions from Hollinger's paper are that observations of microwave brightness temperature of the sea showed a definite dependence on wind speed.

1.5 Previous salinity missions and campaigns

The work affirms that this dependence is due to roughness effects of the surface associated with wind-driven waves, and that it is frequency dependent.

Cape Cod Canal measurements - Swift

C. T. Swift and his team carried out several measurements during a nine-month period, in 1972, at the Cape Cod Canal in Massachusetts (Swift, 1974). A four-frequency microwave radiometer system was installed on a railroad bridge over the Canal, and several ground truth sensors were installed to correlate radiometric data with environmental changes. The antennas operated at frequencies of 7.5, 4.0, 1.4 and 0.75 GHz, performed elevation scans from -23° to 162° with steps of 3° or 6° , and measured the horizontal and vertical brightness temperatures.

The measurements showed that sea surface roughness causes a general increase in the horizontally polarised component of the brightness temperature of about 3 to 9 K, that is weakly dependent on the viewing angle and frequency. Also they observed that for vertical polarisation at 60° the brightness temperature is independent of roughness.

The author presents, also, measurements of specular reflection and scattering of the sunlight. He also explains that foam streaks which, were swept through the beams of the antennas, caused no measurable increase in the brightness temperature, even though he mentions that it is in contradiction with other authors results.

1.5.2 Airborne

Airborne campaigns provide the advantage of performing long distance measurements, allowing the detection of salinity fronts and other spatial variations.

Chesapeake Bay Measurements - Blume

On 24 August 1976, an L and S-band radiometer system (built by NASA Langley Research Center) was installed on one NASA C-54 aircraft and operated in a flight from NASA Wallops Flight Center over the lower part of Chesapeake Bay and adjacent Atlantic Ocean (Blume et al., 1978). This area was selected because the mixing of fresh and salt water results in strong salinity gradients. Some sea truth data were obtained from several locations in the measurement area. Whereas the S-band radiometer was a superheterodine type, the L-band radiometer was a direct-type receiver.

Sea conditions for the measurements were fairly calm with a 3.5 m/s surface wind. The airplane flown at 1.4 Km height and all measurements were nadir

1 General Introduction

observations. The radiometric data were corrected for cosmic and galactic radiation, atmospheric effects and antenna-beam efficiency, but no correction for surface roughness due to wind speed at L-band was included, since they believed it was negligible at this frequency. Some comparison was made between salinity obtained from radiometric measurements and ground truth for several points, and the mean deviation was 0.5 psu with a standard deviation of 0.91 psu.

SLFMR

The Scanning Low Frequency Microwave Radiometer (SLFMR) - also known as salinity mapper- is a 1.4 GHz radiometer designed and built for the National Oceanic and Atmospheric Administration (NOAA). SLFMR has 6 beams located across the flight track, and are oriented at 39°, 22° and 7° off nadir on each side of the plane. The aircraft also carries an infrared radiometer to measure sea surface temperature with a beamwidth equal to the SLFMR.

The system was completed in June 1993 and in August it was mounted on the VIMS aircraft and flown over areas around the southern part of the Chesapeake Bay. The general performance of the system was good, however the data collected by the SLFMR suffered from contamination from man-made Radio Frequency Interference (RFI). Further flights in the same area encountered the same levels of RFI which made impossible to retrieve salinity from radiometric measurements. Afterwards, SLFMR was flown over Delaware Bay, in an attempt to escape from the high RFI. Here, it was experienced annoying, but tolerable amount of RFI at the flight altitude of 609 m. The average difference between the time series of salinity derived from SLFMR and in situ data was less than 1 psu, after applying a 9 point running average to the SLFMR measurements (Miller et al., 1998).

ESTAR

Electronically Scanned Thinned Array Radiometer (ESTAR) was the first prototype built to test a new technology being developed for passive microwave remote sensing: aperture synthesis. This approach permits substantial reduction in the antenna aperture needed for a given spatial resolution.

The radiometer was developed as part of cooperative research at the NASA Goddard Space Flight Center, the University of Massachusetts, and the USDA Agricultural Research Service in Beltsville.

It is an L-band hybrid real-and-synthetic aperture radiometer that employs real aperture antennas to achieve resolution along track and uses aperture synthesis to achieve resolution in the across track dimension (more information in Le Vine et al. (1994)). ESTAR is a H-polarisation radiometer and was designed

1.5 Previous salinity missions and campaigns

for the remote sensing of soil moisture.

A series of measurements called the Gulf Stream Experiment were conducted during summer 1999. The ESTAR radiometer (H-pol) and the SLFMR (V-pol) were placed on NASA P-3 Orion aircraft. Also a C-band radiometer, a scatterometer, and an infrared radiometer were installed in the plane. Surface salinity measurements were provided by thermosalinographs and surface drifters deployed by research vessels. Salinity retrieved with ESTAR was in good agreement with the salinity measurements from the vessels. Similar results were obtained with SLFMR.

PALS

The Jet Propulsion Laboratory (JPL) designed and built a Passive/Active L/S-band (PALS) microwave airborne instrument to measure ocean salinity and soil moisture. The instrument requirements were determined to allow salinity measurements to be made with an accuracy of 0.2 psu over open ocean. This instrument has dual-frequency, dual polarisation radiometers and polarimetric radar sensors, and was installed in a NCAR C-130 aircraft. The antenna is a high beam efficiency conical horn with relatively low sidelobes pointed at 38° incidence angle (Wilson et al. (2001)). The instrument is non-scanning, thus a single-footprint track is sampled along the flight path. An IR temperature sensor was used to measure the changes in sea surface temperature.

The first set of ocean measurements were made in July 1999, southeast of Norfolk VA. over the Gulf Stream, and out into the open ocean. The surface truth measurements of SSS, SST and surface winds were gathered by a ship from Duke University. Measurements demonstrated that PALS is a radiometer with an absolute accuracy <2 K, and a relative stability of ~ 0.2 K over a few hours. A sudden decrease of 0.2 K measured in the brightness temperature corresponded to the salinity increase of 0.4 psu measured by the vessel.

Other experiments were carried out in the summers of 2000 and 2002, and the plane performed seven flights over a buoy off the California coast near Monterey bay. A research ship performed some *in-situ* measurements.

In October and November 2001, PALS radiometer brightness temperature measurements were made from a saltwater pond over a temperature range from 8.5 to 32 °C and salinity from 25 to 40 psu (Wilson et al. (2004)). The study shown that Klein and Swift dielectric model had the best agreement with the saltwater pond data (RMS<0.1 K, which corresponds to a salinity error of <0.2 psu); however, all the models had RMS differences within 0.3 K.

These campaigns were in support of the development of ocean surface salinity remote sensing techniques for the future Aquarius space mission from NASA.

1 General Introduction

1.5.3 Spaceborne

Experiment S-194 on Skylab.

An L-band radiometer (Experiment S-194) was mounted on the NASA Skylab spacecraft and was used to remotely determine soil moisture over various types of terrain, and sea surface salinity content of sea water.

The spacecraft was launched in May 1973; the NASA manned mission extended through February 1974. The Skylab orbit included a mean altitude and inclination of 439 Km and 50 degrees, respectively. In addition, a 5-day repeating orbital period of 93 minutes each was achieved at an altitude velocity of 7.65 km/s.

The L-band radiometer was mounted on the spacecraft's exterior surface to provide a nadir ground footprint of 115 Km. Scientific data was digitally recorded on magnetic tape and subsequently returned to Earth by the on board manned crew.

A self-calibration, Dicke-switched radiometer was developed for reliable unattended operation in deep space, and a fixed planar array antenna oriented towards nadir was used to provide a low-loss and high efficiency transducer with controlled beamwidth characteristics.

The radiometer exhibited temperature sensitivities of less than 0.5 K, and accuracy better than 0.7 K at a source temperature of 296 K for an RF bandwidth of 27 MHz and an integrating time of 1s. In addition, long-term drift was measured to be less than 0.2 K (Flattau et al., 1976).

Table 1.1 summarises the measurements performed until now with L-band radiometers. Some of the campaigns will be largely explained in next chapter.

1.6 Current satellite salinity missions

Currently two space missions are in progress to measure sea surface salinity (SSS) from space. The first one is a mission from the European Space Agency, SMOS, which was approved in 1999 and the launch is planned for 2007. The second mission is AQUARIUS, from NASA, which is planned to be launched in 2008. The nominal life time for both is 3 years, so more than one year of tandem mission will be possible.

1.6.1 SMOS

In 1999, the European Space Agency (ESA) selected the Soil Moisture and Ocean Salinity (SMOS) mission as an Earth Explorer Opportunity mission (Sivestrin

1.6 Current satellite salinity missions

| Campaign/author | year | Meas. Conditions | Incidence angles | polarisation |
|-----------------|-----------|------------------|------------------|--------------|
| Hollinger | 1971 | platform | 20°-65° | H & V |
| SKYLAB | 1974 | Spaceborne | 0° | H & V |
| Swift | 1976 | bridge on canal | 25°-55° | H |
| Blume | 1976 | airborne | 0° | H & V |
| Webster et al. | 1976 | airborne | 0° | linear |
| SLFMR-NOAA | 1993 | airborne | 7°-39° | V |
| ESTAR/SLFMR | 1999 | airborne | 0°-60°/7°-39° | H & V |
| JPL-PALS | 1999 | airborne | 40° | H&V |
| WISE | 2000/2001 | platform | 25°-65° | H&V |
| EuroSTARRS | 2001 | airborne | 0°-75° | V |
| LOSAC | 2001/2003 | airborne | 22°-52° | 4 stokes |
| PLATA | 2003/2004 | airborne | 7°-39° | V |

Table 1.1: Available L-band radiometric data.

et al., 2001, Font et al., 2000). This intended to be a very cost-effective space mission, implemented on short time-scales. SMOS will be launched on February 2007, if no delays occur, and it will have a nominal duration of 3 years (5 expected).

The goal of the SMOS mission is to observe two key parameters, which have never been measured by satellite before: Soil moisture (SM) over land, and sea surface salinity (SSS) over the sea by means of an L-band (1.400-1.427 GHz) microwave imaging radiometer. SMOS will contribute also to the research of the cryosphere, through the assessment of the snow mantle and of the multi-layered ice structure.

SMOS aims at providing, over the open ocean, global salinity maps with an accuracy better than 0.1 psu, every 30 days and 200 x 200 km spatial resolution; over land surfaces, global maps of soil moisture, with an accuracy better than 4% every 3 days with a space resolution better than 60 Km, as well as vegetation water content with an accuracy of 0.2 kg/m² Font et al. (2003b).

SMOS will fly in a sun-synchronous (6 a.m. ascending), near-circular, 755 km altitude orbit, with a revisiting time between 1 and 3 days. The satellite will be

1 General Introduction

put in orbit with a Russian Rockot launcher, and will be carried on a standard 'spacecraft bus' called PROTEUS developed by the French Space Agency, CNES. The total mass of SMOS is 683 Kg.

SMOS is a demonstrator mission, with ambitious scientific objectives, based in an innovative approach and concept: the use of an L-band 2-D interferometric polarimetric radiometer, called MIRAS (Microwave Imaging Radiometer by Aperture Synthesis).

This novel measuring technique permits to SMOS to be the first ever spaceborne mission that will provide global maps of soil moisture and ocean salinity.

Instrument characteristics

MIRAS (Microwave Imaging Radiometer with Aperture Synthesis) is a synthetic aperture radiometer that allows measuring T_B over a large range of incidence angles, for two polarisations (Martín-Neira and Goutoule, 1997). It consists of a central structure with three deployable arms in a Y-shape (see figure 1.12a). Each arm has a longitude of 3.36 m, and carries 21 receivers, within a spacing of 0.88λ . MIRAS has 69 L-band receivers in total (see figure 1.12b).

The antenna will view an area of almost 3000 km in diameter. However, due to the interferometric measurement principle, the Y-shape antenna and the spacing between antenna elements, the field of view is limited to an hexagonal shape area of about 1000 km across (see figure 1.12c). This shape is due to the aliasing effect, which is presented when ambiguities are detected in the measurement of the phase differences.

The nominal spatial resolution is 50 km (35 km at the FOV centre) for a circular orbit of 755 km and 32° tilt angle. At boresight the radiometric resolution for each polarisation will be about 2.4 K (for 1.2 sec integration time), degrading out-of-boresight.

EADS-CASA Espacio, Spain, is the prime contractor for MIRAS. The antenna-receivers, also called LICEF, are developed at MIER S.A., Catalonia, Spain. They use multi-layer 'microstrip' technology to achieve best performance in terms of gain, bandwidth and differentiation of horizontal and vertical polarisation components. Each LICEF antenna weights 190 g, is 165 mm in diameter and is 19 mm high.

MIRAS can operate in two measurement modes - dual-polarisation or full-polarimetric mode. The baseline is the dual-polarisation mode, where all the LICEF antennae will be switched between horizontal and vertical measurements, thus permitting the measurement of the horizontal and vertical components of the received microwaves. In addition, the full-polarimetric mode has been implemented to acquire both polarisations simultaneously. The advantage of this

1.6 Current satellite salinity missions

enhanced mode is that it provides additional scientific revenue, however, the amount of data that has to be transmitted to the ground is doubled. Only in-flight experiences will show whether the dual-polarisation mode satisfies the scientific mission objectives, or whether MIRAS will be continuously operated in the more demanding full-polarimetric mode.

Receiver parameters are sensitive to temperature and ageing. Therefore, they need to be regularly calibrated in flight to ensure that the mission required accuracy is met. Several times per orbit an internal calibration system injects a signal of known characteristics into all the LICEF receivers (they are total power radiometers). In addition, every 14 days an absolute calibration with deep space or celestial target of known signal strength will be performed, requiring the satellite to perform specific attitude manoeuvres.

The radiation emitted by the Earth is measured by each antenna-receiver and transmitted later to a central correlator unit, which performs all the cross-correlations of the signals between all possible combination of receiver pairs. By performing the pre-processing on-board, the amount of data that has to be transmitted to the ground is greatly reduced.

The satellite position and its orientation need to be known at each moment, to properly geo-locate ground targets. These data will be provided by a GPS receiver and by star trackers.

The information will be stored in memories, and transmitted to the ground by a X-band downlink every time the ground station is seen by the satellite.

Multi-angular capability

Thanks to the large field of view of SMOS, as the satellite moves along its orbital path each pixel is observed under several incidence angles, which range from 0° to 55° approximately (see figure 1.12d). This feature is very important, since each snap shot (every 0.3 s) will be independent from the others, so the observations of a pixel from different incidence angles will be independent. This is crucial for the development of new and more efficient retrieval methods (Camps et al., 2002b). Latter, several spatial and temporal averaging can reduce the noise of the measurements.

For each satellite overpass, the spatial resolution of SMOS varies between 30-60 *km*, and the expected accuracy of SSS is about 1 psu.

The Global Ocean Data Assimilation Experiment (GODAE), a pilot experiment set-up by the Ocean Observations Panel for Climate, aims to demonstrate the feasibility and practicality of real-time global ocean data modelling and assimilation systems, both in terms of their implementation and their utility (Smith and Lefebvre, 1997). Following the recommendations of the Ocean Observing Sys-

1 General Introduction

tem Development Panel, the proposed GODAE accuracy requirement for salinity retrieved from satellite data is specified as 0.1 psu for a 10 day and $2^\circ \times 2^\circ$ resolution requirement for global ocean circulation studies. Considering the exploratory nature of SMOS, the GODAE requirement represents a technically challenging objective. It will be possible to average data over 30 days or longer periods for many climate studies and thereby further reduce of the random measurement noise. Monthly averages over 100 km boxes would provide data comparable to the standard climatologies (Levitus et al., 1994). Lower accuracy, higher resolution measurements (typically 0.5 psu, 50 km, 3 days) provide a means to monitor salinity fronts in various regions.

SMOS expects to meet, in some cases, the GODAE requirements, so having SSS measurements with an accuracy of 0.1 psu, for 10 days and over boxes of 200×200 km boxes. For that a large averaging in time and space is needed.

Auxiliary data problem

To retrieve SSS from radiometric measurements other parameters, not measured by SMOS, are needed. The most important are: SST, wind speed, and maybe significant wave height. These parameters, called auxiliary parameters, must be known with good accuracy, since the sensitivities of T_B to them are similar to or larger than the sensitivity to SSS.

In most occasions the SMOS satellite overpasses will not coincide with other satellite sensors sampling the parameters needed. Also numerical and diagnostic models will probably not give a value for the time and position of SMOS acquisition. Under such circumstances, maybe the auxiliary parameters should be estimated somehow in the SSS retrieval algorithms using combined information.

Part of the work presented here is focused on studying how to obtain these auxiliary parameters data, the impact of errors on them to the retrieved salinity, and to analyse which is the best method to be used by the SMOS processing chain.

1.6.2 AQUARIUS

Aquarius is a NASA/Earth System Science Pathfinder (ESSP) mission focused in measuring global Sea Surface Salinity. The mission science goals are to observe and model the processes that relate salinity variations to climatic changes in the global cycling of water, and to understand how these variations influence the general ocean circulation.

The goal of Aquarius is to provide global observations of SSS, covering the Earth's surface once every 8 days, and to deliver monthly 100 km resolution SSS

1.6 Current satellite salinity missions

maps with an accuracy of 0.2 psu.

The instrument, built by NASA, consists of three real aperture L-band polarimetric radiometers and a scatterometer at 1.26 GHz, which will measure the sea surface roughness, a crucial variable to retrieve salinity. The size of the deployable antennas is 3 m x 6 m x 4 m. The footprint sizes are: 62-68 km, 68-82 km and 75-100 km. The spacecraft (SAC-D) will be contributed by Argentina's Comisión Nacional de Actividades Espaciales (CONAE).

In September 2008, Aquarius will begin its 3-year mission on a Delta II rocket launched from Vandenberg Air Force Base in California. The science instrument will be carried into a 600 km sun-synchronous orbit, with revisit time at 6 am/6 pm polar orbit. CONAE will conduct operations, provide command capability and receipt of telemetry and scientific data.

Other instruments on board the SAC-D are: the New InfraRed Scanner Technology (NIRST) camera; the K-band radiometers, which will provide complementary surface temperature measurements, surface winds, rainfall and characteristics of sea ice; and a high sensitivity Optical Camera and the Data Collection Transceptor complete the set of Argentine instruments that shall be designed and built by CONAE with the participation of other scientific organisations in the country. Other possible contributions are: the LAGRANGE instrument of the Italian Space Agency (ASI), devoted to observations of GPS satellite occultations in order to supply information about the atmosphere temperature, pressure and water vapour pressure contents and the SODAD instrument of the French Centre National d'Etudes Spatiales (CNES), for the measurement of the properties of micrometeorites and space debris (more information in <http://aquarius.gsfc.nasa.gov/>).

Many projects have been carried out during the period 2000-2003 to increase our knowledge of the salinity retrieval from L-band measurements, and especially the effects of the different geophysical factors in this retrieval. Several studies and field experiments have been conducted, including those sponsored by ESA during the SMOS extended phase A, by national agencies in Europe, and in the USA in support of the Aquarius/SAC-D mission. Significant progress has been made in many aspects of the problem. Font et al. (2004) makes a review on the clarifies aspects and also the ones which still unclear.

1.7 Objectives and thesis plan

The objective of this thesis is to analyse several aspects of the SSS retrieval process which are still unclear, using several campaign datasets and the SMOS End-to-End Performance simulator. This study is a first step to clear up some of the open questions of the SMOS processing chain.

The thesis treats the emissivity modelling aspect by explaining the different forward models necessary to describe the emissivity of the sea. Latter the state of the art of them is exposed and compared. A new model derived by the author is presented.

The thesis also approaches the problem of the auxiliary parameters. A study of the impact on the retrieved salinity of auxiliary parameters errors has been performed and some possible sources for the roughness parameters has been tested. Finally a new method less sensitive to auxiliary parameters errors, and developed by the author, is exposed.

The thesis organisation is as follows:

- **Chapter 2** presents the field campaigns whose data have been used to perform the study. The first two are largely explained and results exposed, since the author participated very actively in the preparation and results analysis. Other campaigns are shortly described.
- **Chapter 3** describes some of the emissivity models that are best accepted in the literature. A new model derived from campaign measurements that is proposed by the author, is presented in this chapter.
- **Chapter 4** introduces some possible sources of auxiliary parameters that can be used for retrieving SSS from campaign measurements. Their temporal and spatial resolutions are exposed, and a comparison of them in a specific period and area is done.
- In **Chapter 5** the salinity retrieval process from radiometric measurements is performed. First the emissivity models are studied, and results are compared. Secondly different auxiliary sources are tested. A new method for obtaining these auxiliary data is proposed.
- **Chapter 6** uses the SMOS End-to-End Performance simulator to address the same problems that have been addressed in the above chapter by using real data.

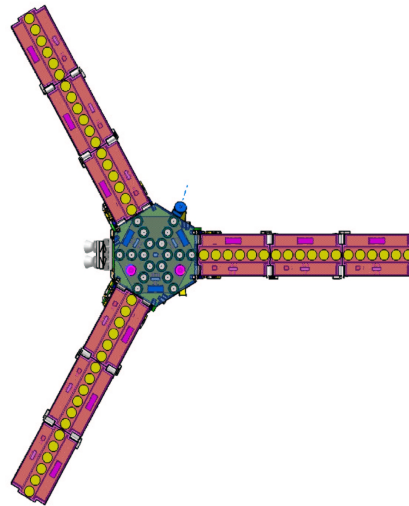
1.7 Objectives and thesis plan

- **Conclusions** on the issues investigated are exposed. Some recommendations are done for SMOS Level 2 retrieval process, and future works are suggested.
- **Appendix A** presents a list of articles and communications on congresses that have been derived from this work. Two peer review articles performed by the author are attached.
- **Appendix B** reviews the inversion methods used in this thesis.
- **Appendix C** presents technical documentation of instruments used in the campaigns where the author has participated.

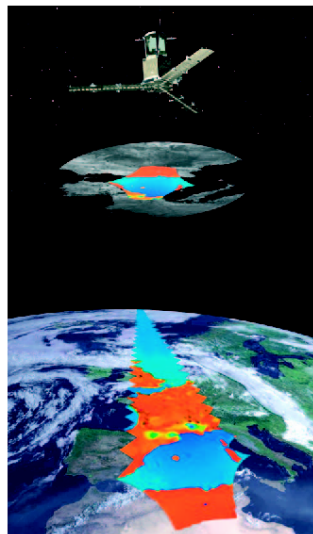
1 General Introduction



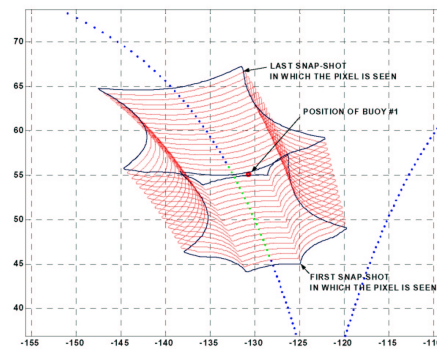
a)



b)



c)



d)

Figure 1.12: a) Artist's view of SMOS (from ESA Medialab). b) Proposed design of the Y-shaped MIRAS radiometer with 18 receivers per arm (from EADS-CASA). c) Field of view of SMOS (from ESA Medialab). d) A single spot (e.g. a buoy) is seen in successive snapshots under different angles and spatial and radiometric resolutions depending on its position within the instrument alias-free field-of-view (from Camps et al. (2002a)).

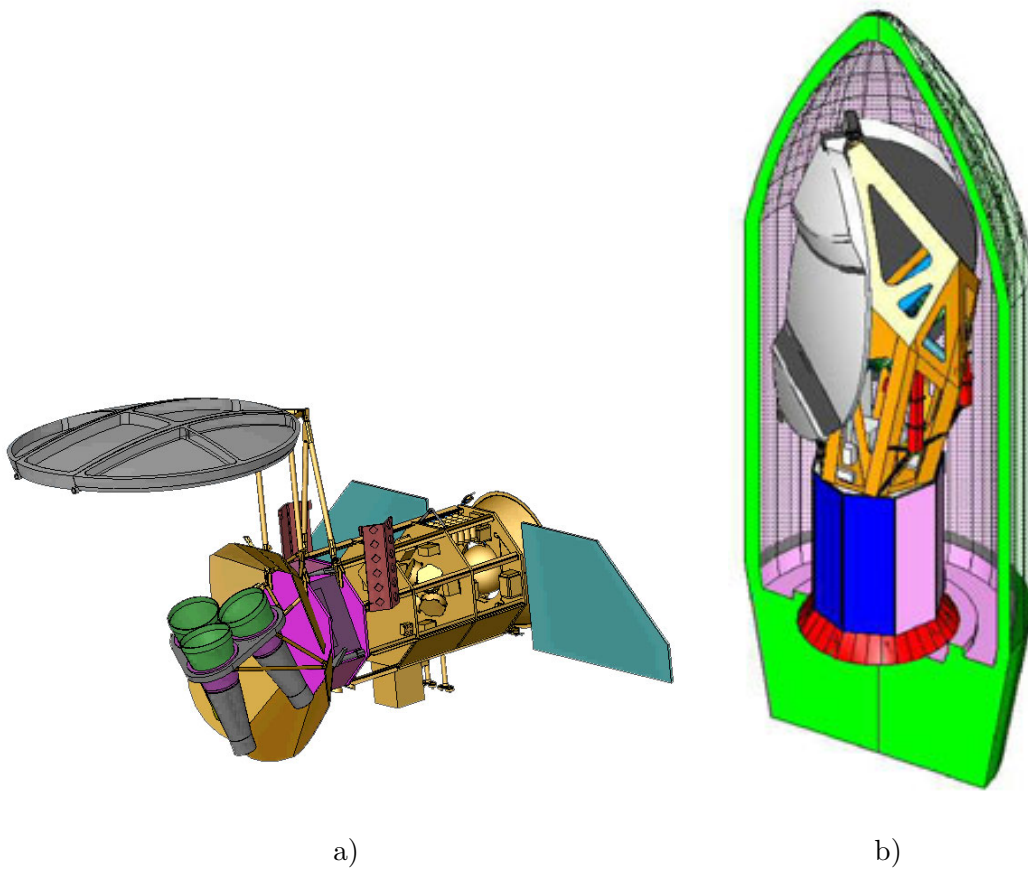


Figure 1.13: a) SAC-D/Aquarius aircraft. b) Aquarius folded into the rocket.

1 General Introduction

Chapter 2

Campaigns

Several dedicated campaign activities were conducted during the feasibility and design phase of the SMOS mission.

WISE 2000 and 2001 were carried out at an oil rig in the North West Mediterranean to examine the relationship between the radiation emitted from the sea surface at L-band under varying sea-state conditions as a result of different wind speeds and direction, different wave types, and varying foam coverage.

EuroSTARRS was an aircraft campaign that carried an L-band radiometer. It was flown over the oil rig area, when WISE 2001 was going on. EuroSTARRS had a similar acquisition as SMOS, and the objective was to measure the influence of some meteorological and oceanographic effects on the measurement of ocean salinity.

FROG 2003 experiment was addressed to understand the effect of foam and rain on the L-band emissivity measurements.

Finally the Plata campaign, consisted in a ship and an airborne survey that was performed at the La Plata river mouth area, where strong gradients on salinity are encountered (South Atlantic).

These campaigns and their results are largely explained in this chapter, since this experimental data is the basis of most of the work done during this thesis. The author has considered that an exhaustive explanation of the experimental campaigns and its results is essential to estimate the quality of the results obtained in this work.

2 Campaigns

Since 2000, the author of this thesis has been working very actively on the preparation, execution and data processing of the WISE and EuroSTARRS campaigns. Those activities had a very long duration (around 1.5 years), so it has been considered that a detailed explanation of them was required in this document.

On the other hand, the author did not participate in the FROG campaign neither la Plata preparation, but their data have been used.

Therefore this chapter has been divided in two sections. The first one will explain, describe and show the results of the two campaign in which the author participated actively. The second section will present the campaign in which the author has not been working, but data has been used in the thesis. Of course the first part will be exposed in much more detail.

2.1 Campaigns with active participation of the author

2.1.1 WISE

The determination of the L-band brightness temperature sensitivities to wind speed and their azimuthal variation were addressed through two ESA-sponsored joint experimental campaign called WISE (WInd and Salinity Experiment) involving 6 research teams from Spain (Universitat Politècnica de Catalunya, Institut de Ciències del Mar - CSIC, and Universitat de València), France (Laboratoire d'Océanographie Dynamique et Climatologique, and Centre d'Études Terrestres et Planétaires), and the USA (University of Massachusetts, as a guest institution during WISE 2000).

The WISE 2000 and 2001 campaigns took place at the Casablanca oil rig, located at $40^{\circ}43.02'$ N $1^{\circ}21.50'$ E, 40 km away from the Ebro river mouth at the coast of Tarragona, Spain. The sea bed is at 165 m depth, and the sea conditions are representative of the Mediterranean shelf/slope region with periodic influence of the Ebro river fresh water plume. WISE 2000 data acquisition spanned from November 25th, 2000 to December 18th, 2000 and from January 8th, 2001 to January 15th, 2001, and WISE 2001 from October 23rd, 2001 to November 22nd, 2001.

The following instruments were deployed: a fully polarimetric L-band radiometer (UPC, Fig. 2.1a), a fully polarimetric Ka-band radiometer (UMass, Fig. 2.1b, only in WISE 2000), four oceanographic and meteorological buoys from ICM and LODYC (Figs. 2.1c, 2.1d, 2.1e and 2.1f; buoy 3 get damaged during mooring in WISE 2000), a portable meteorological station (UPC), a stereo-camera from CETP (Fig. 2.1g) mounted on a handrail and pointing to the North

2.1 Campaigns with active participation of the author

during WISE 2000 and to the West during WISE 2001 to provide sea surface topography and foam coverage, a video camera from UPC mounted on the antenna pedestal (Fig. 2.1a), and a CIMEL infrared radiometer from UV to provide SST estimates mounted on the antenna pedestal during WISE 2000, and on a handrail and pointing to the West during WISE 2001. Additionally, satellite imagery and water samples were acquired.

Figures 2.2a and 2.2b show the location of the instrumentation during WISE 2000 and WISE 2001, respectively. In WISE 2000 the radiometers and the stereo-camera were pointed to the North, in the direction of the dominant winds. However, due to the RFI (Radio Frequency Interference) coming from Tarragona city and probably the Barcelona airport, in WISE 2001, the instrumentation was pointed most of the time to the West, except in the afternoon-evening were it was pointed to the North-East to avoid the Sun. The microwave radiometers and the video camera were mounted on a special terrace built to install the radiometers at the 32 m deck that allowed performing an azimuth scan from 80 W to 40 E and an elevation scan from about 25 incidence angle to an elevation of 140° (when pointing to the zenith the radiometer collected radiation from upper floors and the helipad). The IR radiometer was mounted on the radiometer pedestal during WISE 2000, and on a handrail at the 28 m deck during WISE 2001. The stereo-camera was mounted on a handrail at the 28 m deck. The control room was, also, at the 28 m deck. Figure 2.2c shows a picture of the North side of the Casablanca oil rig indicating the position of the L-band radiometer. The instrumentation deployed is described below:

- L-band Automatic Radiometer (LAURA): The UPC L-band AUtomatic RAdiometer is a fully polarimetric radiometer (Fig. 2.1a) designed and implemented in the facilities of the Department of Signal Theory and Communications (TSC) of the Polytechnic University of Catalonia (UPC) (Villarino et al. (2002)). The antenna is a 4 x 4 microstrip patch square array, with a half-power beamwidth of 20°, measured side lobe levels at E- and H-planes of -19 dB and -25 dB, respectively, a cross-polarisation smaller than -35 dB in the whole pattern, and smaller than -40 dB in the main beam, and a main beam efficiency (MBE) of 96.5% defined at the side lobe level. The antenna pedestal was oriented by computer controlled step-motors and gear-reductions, and the antenna elevation was measured by means of a Seika inclinometer mounted on its back with a resolution $<0.01^\circ$ with a $\pm 70^\circ$ angular range. The radiometer architecture is based on 2 homodyne L-band receivers with I/Q down-conversion. Receiver inputs can be switched between three inputs: (i) the H and V antenna ports and (ii) two matched loads, or (iii) a common noise source. The in-phase components of both channels are connected to two power detectors. The Dicke

2 Campaigns

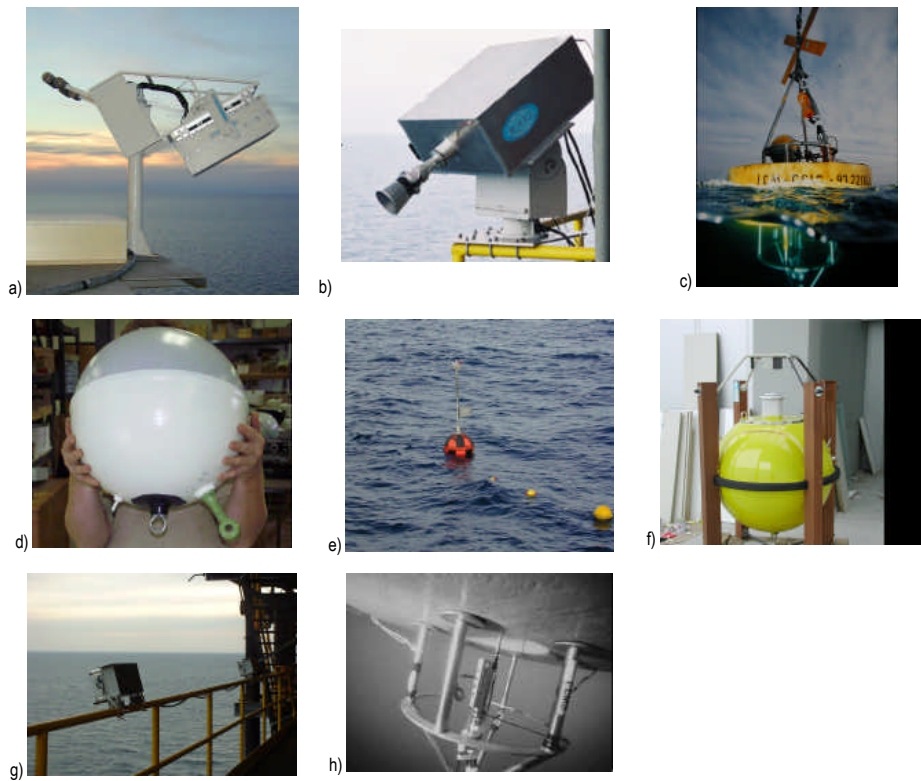


Figure 2.1: Instrumentation deployed during WISE 2000 and 2001: a) L-band polarimetric radiometer (UPC), video camera (UPC) and IR radiometer (UV), b) Ka-band polarimetric radiometer (UMass, only in WISE 2000), c) EMS buoy (buoy 1, ICM), d) Clearwater SVP buoy (buoy 4, LODYC), e) Aanderaa CMB3280 buoy (buoy 2, ICM), f) Datawell wave buoy (buoy 3, LODYC), g) pair of stereo-cameras (CETP), and h) underwater view of the CTD recorder in buoy 1 to sample near-surface salinity.

2.1 Campaigns with active participation of the author

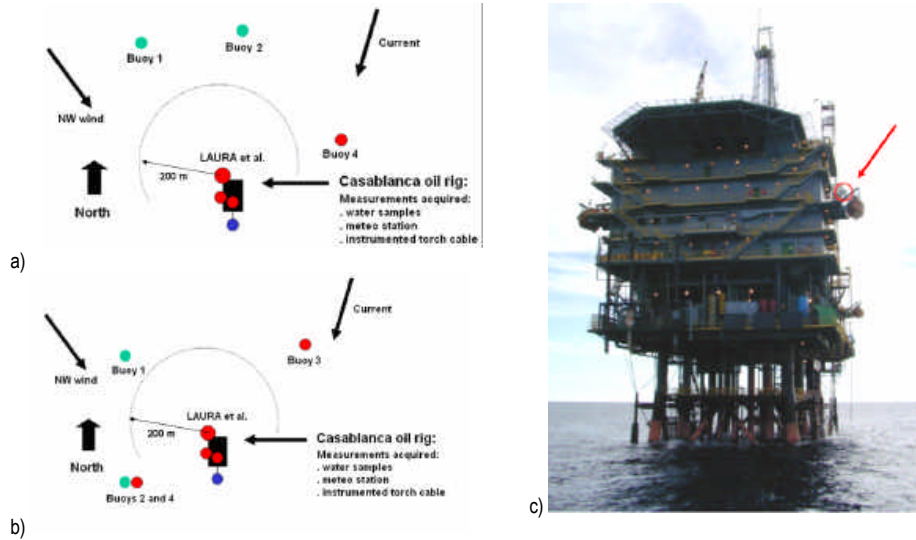


Figure 2.2: Instrumentation and buoy location during (a) WISE 2000 and (b) WISE 2001, and (c) North side of the Casablanca oil rig indicating the position of the UPC radiometer.

radiometers are formed by switching receivers inputs from positions (i) and (ii), and performing a synchronous demodulation. The third and fourth Stokes parameters were measured with a complex digital correlator.

- Meteorological Stations: Rain rate, atmospheric pressure, relative humidity and air temperature at 30 m height were measured by the UPC meteorological station connected to the same radiometer computer. These data were used in the numerical models to estimate the down-welling atmospheric temperature. Additionally, on the Casablanca platform there is an automatic MCV S.A. meteorological station installed on the top of the communications tower, 69 meters above the sea level, including the following sensors: wind speed, wind direction, air temperature, air pressure, and relative humidity. These data were recorded and used only as backup information due to the lower resolution and temporal sampling (15 min). However, they were of crucial importance in the WISE 2001 data processing due to the lost and fatal damage of the buoy sensors during a storm on November 15th, 2001.
- Oceanographic Buoys:

2 Campaigns

The oceanographic and meteorological characterisation of the sea environment during WISE 2000 and 2001 was mainly provided by sensors located in 4 buoys moored at bottom depths from 145 to 175 m in an area restricted to navigation within 500 m around the oil platform and close to the radiometers field of view (Figs. 2.2a and 2.2b). These buoys were specifically deployed for the campaign. Additionally, some extra data were collected from the platform itself. Within the WISE team the oceanographic data acquisition and analysis were performed by ICM-CSIC (buoy 1, buoy 2, instruments on platform, and sea operations) and LODYC (buoy 3 and buoy 4).

– Buoy 1 (Fig. 2.1c)

The objective for buoy 1 was to collect conductivity and temperature data near the sea surface close to the radiometers field-of-view, and send them to a data logging station installed on the platform, using a real time link. The buoy was designed and built for WISE 2000 by EMS Environmental Monitoring Systems S.L., and modified for WISE 2001 mainly to host extra power batteries. It was a toroidal body with an inox steel structure to allocate the signalisation elements (flash, radar reflector, and satellite ARGOS beacon) and the measuring and transmitting instruments. The net buoyancy was near to 400 kg.

The main instrument in buoy 1 was a SeaBird MicroCAT system (model SBE37-SM) (Fig. 2.1h). It allows recording in a RAM water temperature and conductivity for further salinity determination. An RS-232 interface allows real-time data transmission by an external UHF link. An additional submersible pump was added to ensure a constant water flow through the conductivity cell. The water inlet was situated at 20 cm below sea level in the central part of the toroid, to minimise the effect of waves (possibility for air bubbles being introduced into the measuring cell).

Temperature and conductivity sensor characteristics are summarised in table B.1 from appendix B.

This allows computing salinity, according to established standards (UNESCO (1978)), with 0.003 psu/month stability, and 0.0002 psu resolution. It has to be noticed that the conductivity cell is equipped with a chemical poison device to avoid biofouling, and the corresponding degradation of the conductivity measurement.

One of the conclusions from WISE 2000 (see below) was the need to increase the quality of wind speed measurements for use in emissivity models improvement. For WISE 2001 a Doppler ultrasonic anemome-

2.1 Campaigns with active participation of the author

ter model 5010-0005 from USONIC, UK was added to buoy 1. This instrument provides a better sensitivity to wind speed (especially at low speeds) than the traditional rotor anemometers and avoids their possible mechanical problems.

It measures wind speed every 0.3 second and transmits it in real time by a standard RS-232 interface. Wind direction measurements were not used, since the anemometer was installed on a moving platform (moored buoy) without any extra compass for absolute direction determination. The sensor characteristics are summarised in table B.3 in appendix B.

A microprocessor, programmed by the author of this thesis, received data from the anemometer every 10 s, collected this data stream together with the MicroCAT data received every 2 min., and sent the whole data set every 30 min., via a radio modem, to a receiver placed in the platform. Additionally, the microprocessor averaged the anemometer data every 30 s and stored them in a RAM. A diagram of data acquisition and transmission in this buoy, as well as the specifications of the microprocessor are added in appendix B

– Buoy 2 (Fig. 2.1e)

The objective was to characterise the sea surface state in the field-of-view during radiometer measurements. Buoy 2 was a standard Coastal Monitoring Buoy (CMB3280) from Aanderaa Instruments, Norway that includes a meteorological station, a significant wave height and period recorder (accelerometer), and an acoustic surface (1 m) current meter. The main floating body has a "wet" diameter of 90 cm and a total buoyancy of 345 kg. The buoy carries security elements (flash, radar reflector), is powered by solar panels, records data internally, and transmits them by VHF in real time.

A high sampling rate produces rapid power consumption and miss functioning of the whole system after a few days. To avoid this, the current meter and the air pressure sensors (both not crucial and highly power consumers) were disconnected.

The remaining parameters recorded by the buoy were: Wind speed, wind direction, air temperature, solar radiation, relative humidity, wave height and wave period, and the accuracy of those measurements are summarised in table B.4 in appendix B.

– Buoy 3 (Fig. 2.1d)

A Spear-F Datawell waverider buoy was provided by LODYC to record the surface wave spectrum in 14 frequency bands every 3 h and transmit it via satellite (Argos system), following the procedure used by

2 Campaigns

MétéoFrance. In addition it transmits the significant wave height and the dominant period of waves. In WISE 2000 the buoy was damaged when trying to deploy it under rough seas, and could not further be used. In WISE 2001 it operated successfully during the entire campaign.

– Buoy 4 (Fig. 2.1f)

A redundant surface temperature and salinity measurement was obtained from a Clearwater SVP small float equipped with FSI temperature and conductivity sensors that were also transmitting data, measured once per hour, via satellite. The expected accuracy at sea is 0.1 psu and 0.1°C for salinity and temperature respectively. In WISE 2000 this float was moored separately, but was lost after one month of operation. In WISE 2001 it was attached to buoy 2 line with a 10 m long iron cable protected with a semi-rigid plastic cover. The buoy 4 satellite Argos beacon was then also used as an extra security element for buoy 2.

The deployment of buoys was difficult in 2000 due to limited availability of adequate ships, and mainly to bad weather conditions. In WISE 2000 only buoy 4 could be moored at the beginning of the experiment (November 15th). The sensors at the platform could be installed on November 29th, and buoys 1 and 2 moored on December 2nd, although part of buoy 2 sensors were not operational until December 13th due to a technical failure. Additionally, the wind speed sensor on buoy 2 did not work for 14 days during the second half of December. As previously said, buoy 3 could not be deployed. The wind sensors on the platform were operational from November 14th. Buoy 4 was lost by mid December, probably after being trawled by a ship. Buoys 1 and 2 were recovered on January 20th, while the instruments on the platform were disassembled on 14 and 15 January, after completion of the experiment.

In WISE 2001 the buoys deployment was made without problems on October 4th from the CSIC research vessel García del Cid, except buoy 1 that was not ready until October 23rd, just at the beginning of the experiment. The instruments on the platform were installed on October 24th. On November 15th a violent storm (easterly wind bursts higher than 120 km/h) occurred on the Casablanca area with maximum waves over 12 m. It was the strongest storm ever recorded in the platform since it was installed in the early 80s, and produced serious damage to its structure. It partially destroyed buoy 2 (that ceased operating and lost stored data) and the anemometer on buoy 1. The link that attached buoy 4 to buoy 2 was

2.1 Campaigns with active participation of the author

broken, and the float drifted away until it could be rescued 230 km south. On November 22nd the buoys were recovered and the instruments on the platform disassembled.

- Measurements from the platform

To complement the oceanographic measurements made by the moored buoys, an extra instrument was deployed on the platform itself. A winch with a hydrographic cable available in the southern side of the platform, hanging from the structure of a gas torch at some 40 m above sea level allowed deploying instruments at any depth.

Using this cable a second SeaBird MicroCAT (without additional pump) was located at 5 m below sea level. The purpose was to record temperature and conductivity at a depth that will be the standard for in situ data to be used for SMOS salinity data validation (e.g. Argo profiling floats). The comparison between the time series recorded by the two identical instruments provided valuable information for the future SMOS data validation strategy. During WISE 2000 the winch was operated in several occasions to obtain vertical T, S profiles in the top 0-5 m. In 2001 this option was discarded as it resulted to be of poor use, the operation was not easy, and produced interruptions in the 5 m time series.

In 2000 an Aanderaa RCM9 Doppler currentmeter was also hung from the cable to record water velocity (plus temperature and conductivity) at 2 m below sea level, as substitution for the sensor that had to be disconnected in buoy 2. This information intended for air-sea flux computations resulted of no further use, and was not implemented in the 2001 campaign.

To check for possible drifts in the conductivity sensors, water samples were taken when deploying and recovering the buoys for later salinity determination with a Guildline Autosol salinometer (performance characteristic in appendix B). These instruments, when used under strictly controlled room conditions, can provide the best salinity values by comparing the relative conductivity of the sample to a reference standard water of 35.0000 psu. The absolute accuracy is 0.002 psu and the resolution 0.0002 psu.

The sampling rate for the data acquisition system on buoys 1 and 2, and the MicroCAT hung from the platform, was set at 2 minutes. This was the minimum allowed to keep all the sensors working properly with enough power available for 2 months of operation. After calibration and cross-comparison of all the deployed instruments with water samples analysed on the laboratory, we can conclude that the recorded temperature and salinity values are correct within 0.02 °C and 0.02 psu, a sufficient quality for the

2 Campaigns

WISE objectives. An exception to this is the conductivity sensor in buoy 4 that produced an underestimation of salinity of around 0.15 psu.

- **Stereo Camera:** The system consists of two digital video cameras Canon Powershot 600 (832x624 pixels), spaced 4 meters and located at 28 m over the sea surface, just below the radiometers terrace (Fig. 2.1g). During WISE 2000 they were pointed to the North, where the radiometers were supposed to point most of the time (upwind direction of dominant winds). However, during WISE 2001 they were pointed to the West, as it was the radiometer to avoid RFI. Of course, to avoid Sun glitter with this orientation, measurements with the stereo-camera were restricted to the morning. Systematic measurements coincident with the radiometer were performed every day from 9 AM to 10 AM. The stereo-camera provides sea foam coverage estimates and sea surface topography, by observing the sea surface from an incidence angle under two different views.
- **Video Camera:** A video camera (8.5 mm lens, auto-iris, resolution 512 x 582 pixels, field of view: 35.6° in horizontal and 25.2° in vertical) was mounted in the antenna pedestal (Fig. 2.1a) to provide an instantaneous view of the sea surface being measured by the radiometer. Images were stored every second. The analysis of the images restricted to a 20° field of view (coincident with the antenna beamwidth) have been used to evaluate the sea foam coverage as a function of wind speed (by analysis of the image histograms), to make an estimate of the sea foam emissivity by comparing the instantaneous sea foam coverage and the instantaneous brightness temperatures (T_h and T_v), and disregard erroneous measurements when the security vessel that makes circles around the platform, birds, or even whales pass through the antenna beamwidth.
- **Infrared radiometer:** The CIMEL CE 312 thermal-infrared radiometer is a four-band radiometer covering 8-13 μm , 11.5-12.5 μm , 10.5-11.5 μm , and 8.2-9.2 μm , with radiometric sensitivities 0.008 K, 0.05 K, 0.05 K, and 0.05 K; and radiometric accuracies 0.10 K, 0.12 K, 0.09 K and 0.14 K, at 20°C, with a field of view of 10°. It was used to provide sea surface temperature estimates, simultaneous with LAURA's measurements. During WISE 2000 the CE 312 was mounted on the LAURA pedestal (Fig. 2.1a) to observe the sea surface with identical conditions (zenith and azimuth angles). However, since the CE 312 read-outs are brightness temperatures, these data have to be corrected for the atmospheric and sea emissivity effects, before being compared with the SST estimates from the AVHRR and the oceanographic buoys. This means that the IR radiometer needed to point to incidence angles larger than 90° more often than the LAURA radiometer in order

2.1 Campaigns with active participation of the author

to measure the down-welling sky radiance. To overcome this conflict, and taking into account that the best SST estimates were found for the lowest observation angles, in WISE 2001 the IR radiometer was mounted alone on a handrail pointing to the sea (West direction) with an observation angle of 25° and the down-welling sky radiance was simulated using the MODTRAN 4 radiative transfer code.

- Satellite imagery and other data:
 - QuikSCAT Wind speed data. Measurements of the NASA satellite-borne QuikSCAT scatterometer (nudge algorithm) at 25 km resolution co-located with the platform using a radius of 0.27° latitude and 0.37° longitude were collected. During WISE 2000 and 2001, 196 and 74 measurements were found, respectively. Since the scatterometer cannot approach closer than 50 km from the coast there were not measurements coincident with the platform: all of them were East and South. These wind speed data were averaged for each satellite pass and the resulting averages were compared with one-hour average of the in-situ measurements. The accuracy at global scale is about 2 m/s.
 - AVHRR SST data. LAC images of the AVHRR instrument at 2 km resolution were recorded and processed by the SATMOS data center (Service d'Archivage et de Traitement Meteorologique des Observations Spatiales, Météo-France/ CNRS). Many images were cloudy. During WISE 2000 the Ebro plume was observed, but not during WISE 2001.
 - ARPEGE wind speed data. Surface wind speed from the analyzed surface fields of ARPEGE, the meteorological model of MétéoFrance, have been co-located with the Casablanca Platform. The resolution of the model is 25 km, 6 h. The co-location radius is the same as for QuikSCAT, that is 0.27° latitude and 0.37° longitude, resulting in nine grid points co-located for each field. The data are from October 1st to November 30th, 2001 and the format is the same as QuikSCAT.

WISE 2000 buoy data analysis

The resolution, accuracy, and hence consistency, between all sensors were good enough to provide the required temperature and salinity data set and reconstruct time series to complement the radiometer measurements.

The surface temperature temporal evolution was typical of the autumn season. November is usually the month when the erosion of the summer stratification is speed up by the occurrence of strong and cold winds: SST values that can be

2 Campaigns

above 25°C at the end of the warm season (September) will drop to around 13°C after completion of the winter vertical mixing (February). In total SST ranged from 17.5° to 14°C (Fig. 2.3). Sea Surface Salinity remained always near 38 psu (Fig. 2.3), a value typical of the Mediterranean open sea waters that, unlike temperature, do not display a clear seasonal salinity signal. This means that the WISE area was usually out of the direct influence of the Ebro river discharge. The salinity time series shows the occurrence of some low SSS events that typically had a duration of 5-6 days. These events, especially the one around December 12th (strongest SSS drop), are associated to similar SST decreases, a possible indication of the river plume reaching the Casablanca area, as continental waters are not only fresher but also colder than ambient water. This interpretation has been confirmed by the sequence of satellite infrared images that display the evolution of the cold-water tongue from the river mouth to this offshore location.

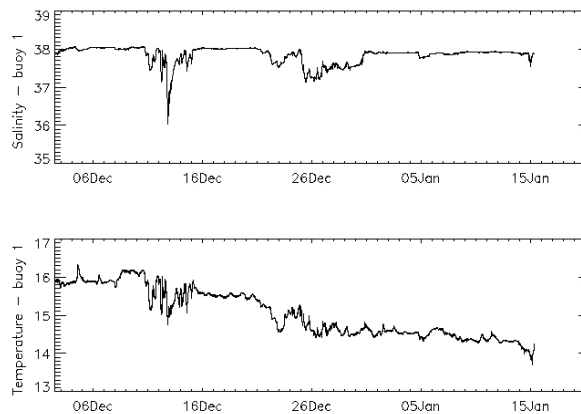


Figure 2.3: Surface salinity and temperature recorded by buoy 1 during WISE 2000.

The two main events detected in WISE 2000 resulted in recorded SSS values 2 psu (December 12th) and almost 1 psu (December 25th) lower than the regular 37.9-38 psu observed all around the experiment.

An important issue related to salinity remote sensing is the possible presence of a vertical salinity gradient. A microwave radiometer will only measure the very surface values, which is not the case of in situ sampling, where sensors have to be completely immersed in seawater. Validation of SMOS salinity determinations will strongly rely on in situ measurements made from standard moored or drifting buoys, or even hydrographic casts or underway measurements from research or opportunity vessels. In all these cases temperature, and especially conductivity,

2.1 Campaigns with active participation of the author

sensors are not operated close to the surface to avoid interference from air bubbles and even to protect them from possible sources of dirt. A present standard value for near surface salinity measurement is 5 m below sea level. In some cases, especially after strong rainfall when the wind speed is low, salinity at this depth can be significantly different from SSS and then errors can be introduced by comparing both values.

The difference between salinity close to the surface (-20 cm, buoy 1) and at 5 m was monitored during WISE by deploying a second instrument at this depth.

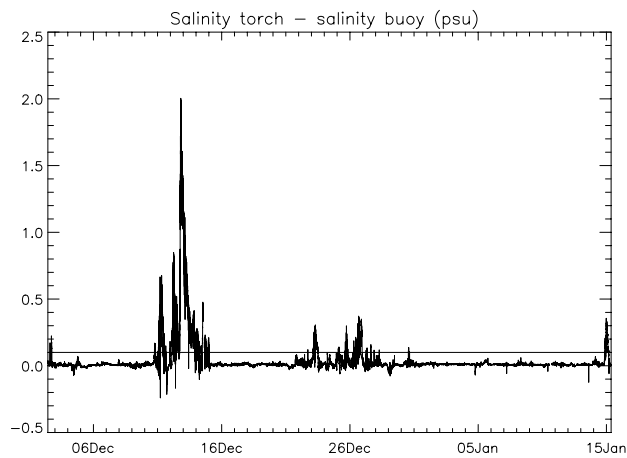


Figure 2.4: Salinity difference between sensors located at -5 m and -0.2 m.

Most of the time the difference between both time series is below 0.1 psu (Fig. 2.4), a value that can be considered a threshold for SSS satellite remote sensing resolution. It is only remarkable during the reported low salinity events, especially that of December 10-15 when the difference reached up to 2.0 psu. The latter is another confirmation that this event was due to an intrusion of the river plume, a near-surface phenomenon, since at 20 cm the salinity drop from ambient water was almost 2.1 psu while at 5 m it was only 0.8 psu maximum.

To increase the knowledge on the vertical resolution of the salinity gradient the sensor at -5 m was manually raised to -2 m, -1 m and to the surface in several occasions. The resulting profiles, with typically a duration of about one hour and a half, display very small salinity variations (usually less than 0.01) except those on December 12th and 14th (low salinity event) and January 10th at surface (probably effect of air bubbles) that can reach up to 0.3 psu. In these specific cases it is remarkable the high temporal variability of the salinity values, which reflects the dynamic behaviour of the event. This was also observed in the SSS time series, where changes of the order of 2 psu can be recorded in very few hours.

2 Campaigns

This poses an additional problem to the satellite SSS validation that has to be analysed in the framework of the general cal/val strategy and considering the decorrelation scales at open oceans.

Wind data, from both buoy 2 and the Casablanca tower, were mapped to 10 m for standard analysis. The hypotheses of neutral stability was checked for the periods where air temperature was available. In general the atmosphere appeared to be slightly unstable.

The wind speed averaged during the whole period is 6.8 m/s. Wind speeds higher than 15 m/s were observed during few days. Unfortunately the strongest winds were observed during the Christmas period during which the radiometer manned experiments were not operating. Wind direction was mainly from the W and NW, with few events from open sea (SE, E or NE). The strongest speeds correspond always to northwesterlies.

The data gathered by the two instruments, mapped to 10 m height was compared, during the period of common measurements. For the comparison to be meaningful the measurements were averaged during one hour. Figure 2.5 shows data from the meteorological station on the platform against simultaneous data from buoy 2. The measurements in the range 3 - 15 m/s (most commonly observed wind speed range and optimal range for instruments) and in the whole data range were fitted.

In the range 3-15 m/s the equation of the fit is: $U_M = 1.09U_B + 0.07$, where U_M is the meteorological station measurement and U_B is the buoy measurement, with an explained variance of 92%. In the whole range it is $U_M = 1.17U_B + 0.20$ with an explained variance of 96%. The mean difference between the instruments is $U_B - U_M = -0.92$ m/s with a standard deviation of 1.83 m/s (Font et al. (2003a)). In the most commonly observed range the instruments differ by about 10%, the standard deviation of the difference being rather high. It was checked that the measurements were nevertheless usable for emissivity models study. This discrepancy might be due to several factors:

- different instruments
- different height: the mapping to 10 m is not perfect and from 69 m it is a large correction (atmospheric stability corrections did not improve the result), the platform is likely to disturb the air flow less at the top than at low altitude.

To compare with the future SMOS situation, when wind data will be needed from other sources, spaceborne wind information has also been analysed. Measurements of the QuikSCAT satellite scatterometer (nudge algorithm) were co-located with the platform. These data were averaged for each satellite pass and

2.1 Campaigns with active participation of the author

the resulting average was compared with one-hour average of the in-situ measurements. The QuikSCAT data have been compared to the meteorological station measurements at 10 m height. The equation of the fit in the range 3-15 m/s is: $U_Q = 0.97U_M + 0.68$, where U_Q is the QuikSCAT measurement, with an explained variance of 74%; the mean difference between the instruments $\langle U_M - U_Q \rangle$ is 0.44 m/s with a standard deviation of 2.8 m/s. The points are rather dispersed, probably due to the imperfect co-location, but they compare rather well. The three wind speed data series (buoy 1, tower station and QuikSCAT) are presented in Fig. 2.6.

During the five weeks when significant wave height (average of the highest third of the waves) could be recorded, data ranged from 0.1 to 4.0 m, with an average of 0.9 m. Wave periods ranged from 1.6 to 7.5 s, with an average of 3.2 s. Most of the time wave height is correlated to wind stress, however, some times during WISE 2000 considerable wave heights were recorded without simultaneous high wind. This is an indication that the wave field at the Casablanca site was at that moment not originated by local winds, but arrived there from other areas (swell). This is also an important issue to be solved for SMOS salinity retrieval if wind speed information has to be used in the computation.

2 Campaigns

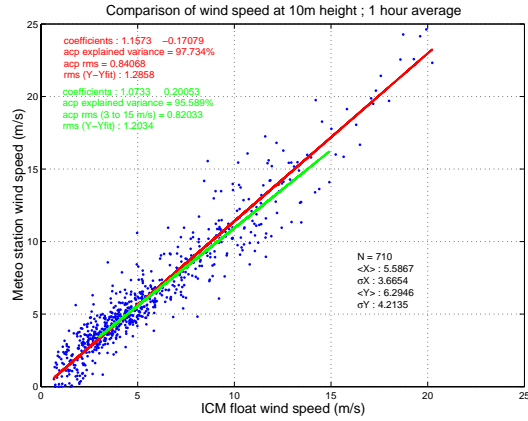


Figure 2.5: Wind speed (at 10 m) comparison for the two in situ data sources during WISE 2000 (from Drange et al. (2001)).

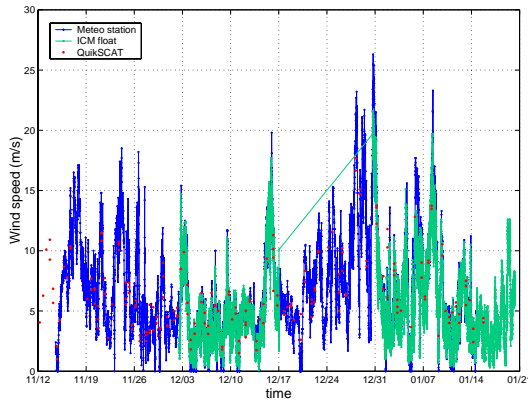


Figure 2.6: Integration of the three wind speed data sets obtained for WISE 2000 (from Drange et al. (2001)).

WISE 2001 buoy data analysis

The 2001 campaign took place also in autumn, but almost one month in advance with respect to the previous year. As previously said, and after the experience gained with WISE 2000, the buoys deployment was made more efficiently using a research vessel, and all the buoys were in place before the beginning of the radiometer measurements. The data intercomparison and analysis was made

2.1 Campaigns with active participation of the author

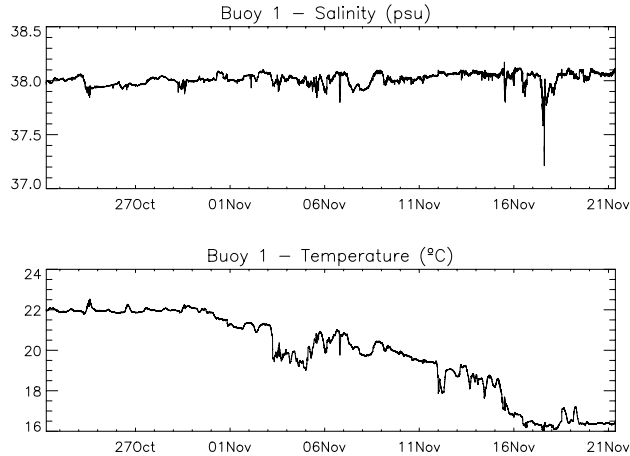


Figure 2.7: Surface salinity and temperature recorded by buoy 1 during WISE 2001.

following the same procedure described for WISE 2000.

At the beginning of the period, the temperature (Fig. 2.7) was still slightly above 22, and did not initiate a clear decrease until early November. A cold event (a drop of almost 2 °C) occurred on 4 November, but after two days the temperature recovered and continued the slow decreasing trend. After the storm of November 15th the decrease was accentuated and by the end of the campaign the temperature was quite stable around 16 °C, practically the same value observed the previous year at that date.

Salinity was very constant around 38.0 psu (Fig. 2.7). Only in 8 short occasions (usually few minutes) during the 30 days period the values differed from this mean by more than 0.1 psu, the expected threshold for salinity detection by SMOS. And just twice the difference was above 0.2 psu, the most remarkable on 18 November (down to 37.2 psu) after an intense rain event.

The vertical structure of salinity near the surface is still more homogeneous than in WISE 2000 (Fig. 2.8). The difference between the values measured by the sensor situated at -5 m and the sensor close to surface overpasses 0.1 psu in few occasions and always during few minutes. Only once, during the rain event mentioned in the previous paragraph, a significant difference persisted for 4 h and reached a maximum of 0.7 psu.

The same wind data analysis as performed in WISE 2000 was applied to the 2001 records. We expected to have better quality data with the ultrasonic Doppler anemometer added to buoy 1, but unfortunately several technical problems reduced the usable information to only two short series. It was due mainly

2 Campaigns

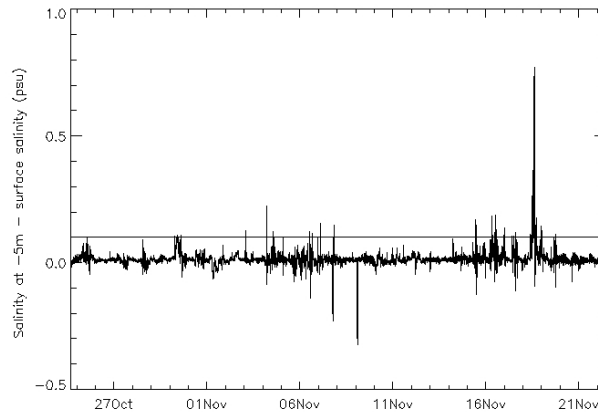


Figure 2.8: Difference in psu between salinity recorded at 5 m below sea level (platform) and at 20 cm (buoy 1) from 23 October until 22 November 2001.

to malfunctioning of the microprocessor that controlled the anemometer data acquisition and transmission just 2 days after deployment. And when this problem could be definitively fixed, the violent storm destroyed the instrument after 6 days of correct operation.

In Fig. 2.9 we present the reconstructed wind speed data series from the different instruments from 4 October (buoys deployment) until 22 November (end of the experiment). The direction was very variable until early November, with two events of strong winds from NE and one from SW. After that, while increasing notably the speed, it was usually from the N and NW with storms (more than 20 m/s) every two days from 9 to 15 November, and all of them from NW except the 'big one' that was from E. After a last minor storm on the 17, the tendency was to lower the speed until the end of the experiment.

Unlike what happened in 2000, during WISE 2001 the radiometer measured under really intense wind and rough sea conditions. Especially remarkable were the two severe storms that occurred on November 11th and 15th. As previously said, the second one produced serious damages to the buoys and to the Casablanca platform structure. Although it was not possible to keep the radiometer working continuously during the storms, data could be recorded under very rough seas.

Fig. 2.10 shows the recorded wave height (four times the variance of the wave slopes), that overpassed 6 m during several hours in both storms, and the peak wave period recorded by the waverider buoy during the whole duration of WISE 2001. It has to be recalled that the spectral wave height (3 h average) recorded by buoy 3 is by definition square root of 2 higher than the significant wave height

2.1 Campaigns with active participation of the author

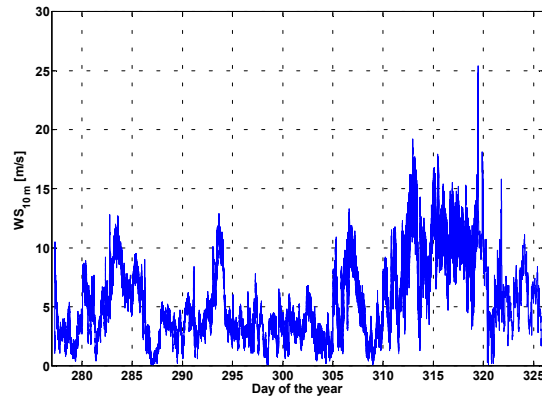


Figure 2.9: Complete wind speed series (mapped to 10 m) measured during WISE 2001.

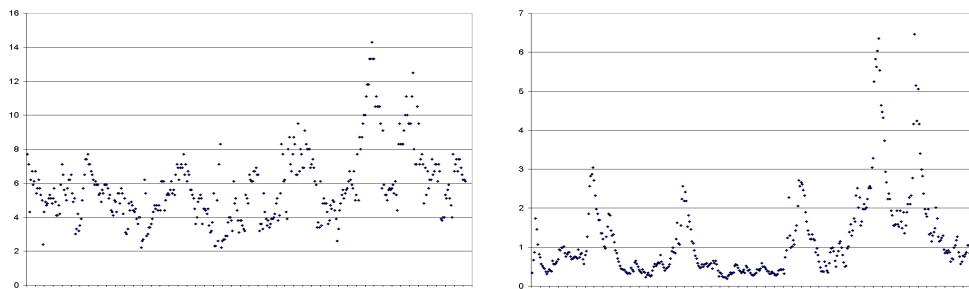


Figure 2.10: Three hours average wave height (left, m) and peak wave period (right, s) recorded by buoy 3 during WISE 2001, from October 4th to November 22nd.

2 Campaigns



Figure 2.11: STARRS instrument installed on a DLR plane.

recorded (every 2 minutes) by buoy 2.

2.1.2 EuroSTARRS

The EuroSTARRS campaign was also sponsored by the European Space Agency (ESA) and the objective was to provide data for the scientific studies supporting the SMOS mission. In particular it acquired 'SMOS like' (in the sense of simultaneously multi-angular) data to advance the knowledge of the passive microwave multi-incidence observations at L-band for various surface types.

The STARRS L-band radiometer is owned by the *Naval Research Laboratory* (NRL), USA, and was available for use by the EuroSTARRS campaign between November 17th and 23rd 2001. The instrument was installed on board a Dornier 228 aircraft from the *German Aerospace Center* (DLR) (see figure 2.11). STARRS instrument has 6 antennas that measure at V-polarisation, only. The radiometer was tilt 12°, respect to nadir when mounted in the plane, to achieve more varied angle measurements, permitting to acquire data at incidence angles of -26.5°, -9.0°, 5.5°, 19.5°, 34.0° and 50.5°.

Data acquired by EuroSTARRS was intended to help to improve the scientific understanding of emissivity in relation to different surface characteristics for retrieving ocean salinity and soil moisture fields. EuroSTARRS was simultaneous to WISE2001 experiment and to the acquisition of data from a dedicated oceanographic research vessel.

Different land surface sites were selected in Europe, and two salinity sites where chosen. One site was Bay of Biscay, around the French meteorological Gascogne Buoy, to study the effects of strong changes in salinity from the coast to the inner part of the Atlantic Ocean. The other site was around the Casablanca oil rig, near the mouth of the Ebro river (Tarragona), mainly to study the effect of

2.1 Campaigns with active participation of the author

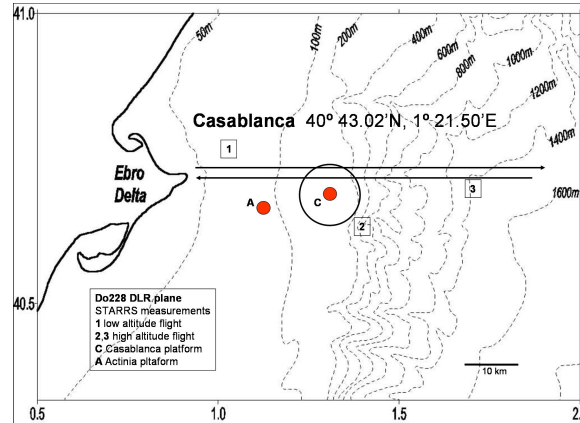


Figure 2.12: EuroSTARRS Casablanca campaign area. Plain and ship path.

wind speed on the salinity measurements and to investigate azimuth dependence.

In the Casablanca area, the flight acquisition plan consisted in three phases. The first one was to draw a transect from the coast near Ebro Delta towards the Casablanca platform (40 km) and until the continental slope (100 km) at 1640 m height (fig. 2.12). This transect was selected to avoid interferences from the platform. The second phase, consisted of performing 10 circles at a constant bank angle of 22° at 278 m height. Given the 12° tilt of the antenna mounting, a range of angles from 4.5° to 72.5° is obtained. The last phase was the reverse course along the first transect and flown at 278 m. The measurements were made after sun shine, in order to avoid the interference from sun glint.

The Institut de Ciencies del Mar (ICM) participated actively during the flight over the Casablanca oil rig, on the November 21st. Simultaneously to the airborne flight two kind of measurements were made at the area. First, the CSIC Research Vessel, 'García del Cid' carried out a survey in a rectangular area extending from 1° to 2° E around the Casablanca platform on November 21st-22nd (fig. 2.12) coincident with the plane overflight on November 21st late afternoon. The oceanographic data collected were:

- Underway near surface temperature and salinity records following the flight line.
- Vertical salinity and temperature profiles spread across the rectangular site measurement area.
- Acoustic Doppler current profiles (ADCP)
- An on-board meteorological station was operating in a continuous mode.

2 Campaigns

The second data set was obtained from sensors installed in buoys moored close to the platform and in the platform itself from the simultaneous WISE 2001 experiment.

The R/V 'García del Cid' left Barcelona on November 21st at 7:00 h and arrived to the Casablanca measurements area at 12:00 h. The underway near-surface measurements were completed on the November 22nd. The analysis of the sea surface fields and the vertical structure can be found in Emelianov et al. (2003).

During the STARRS flight the wind speed in the area was very low, between 3-5 m/s, and direction veering continuously from 75° to 50°. This low wind speed, did not allow to analyse the azimuthal effect.

A strong source of interference was identified when the antenna was pointing towards the city of Barcelona. These interferences make the data not useful during the periods when the antenna was pointing at that direction.

Vessel measurements brought the following conclusions:

- Both temperature and salinity near surface presented a small spatial variability across the sample area, with means values of 17 °C and 38.05 psu.
- Vessel underway high horizontal resolution sampling allowed observing that the temperature spanned over a range of 1.4 °C and the salinity, much noisier, only over 0.3 psu.
- The main gradients were found in the onshore-offshore direction, the same followed by the flight.

2.2 Other campaigns

2.2.1 FROG 2003

The FROG (Foam, Rain, Oil slicks and GPS reflexions) campaign took place in the IRTA (Institut de Recerca i Tecnologia Agroalimentàries) facilities, located in the Ebro River Delta in the south of Catalonia, from March 13th to May 5th. The main objectives of FROG 2003 campaign were the following:

- Acquisition of radiometric measurements of an artificially generated foam covered water surface.
- Acquisition of foam vertical profile snapshots, and measurement of the main parameters to describe the foam by theoretical models.
- Acquisition of radiometric measurements of an artificially generated-rain.

- Acquisition of radiometric measurements of a water surface covered by an oil slick.

This campaign was organised and lead by the Polytechnic University of Catalonia (UPC) team, with collaboration of the University of Valencia for IR measurements.

To achieve these objectives, a pond of 3 m × 7 m dimensions was utilised. The instruments used were: the LAURA L-band full-polarimetric radiometer (the same radiometer used for WISE), a portable meteorological station to measure the atmospheric pressure, temperature, relative humidity and rain rate. Two video cameras were mounted, also, to measure foam coverage and foam vertical profile. Finally a water roughness meter and a water conductivity meter were also installed. An infrared radiometer was placed to measure the SST of the sea water. Figure 2.13 shows the instrument set-up.

To generate the foam, an array of 104 air diffusers was mounted in the pool floor, allowing to regulate the air flux, with a maximum of 500 m³ per hour.

To generate a controlled rain fall a matrix of 14 diffusers were distributed along 3 rows (6 m long, 1.5 m wide) and was mounted on a crane at a maximum height of 13m above the water surface, from where the water drops reached the limit velocity before splashing in the water pool. This set-up generated an equivalent rain rate of approximately 4000 mm/h.

To minimise the radiation coming from buildings and atmosphere, the pool was surrounded by a metallic net. Another effect to consider was the galactic noise, and to minimise this contribution, the radiometer was pointed to the north. To avoid the sun glitter effect, all the measurements were acquired during night-time.

The measurements were done in elevation scans from 20° to 55°, with steps of 1° or 5°, depending on the objective of the measurements. All measurements were repeated in a wide range of salinities from ∼ 0 to ∼ 34 psu in steps of 5 psu, obtained by mixing sea water with fresh water.

Calibration was performed at the beginning and at the end of each measurements cycle (less than 100 min). It consisted in measuring a hot load (microwave absorber) and a cold load (sky) during two hours at each position.

For further information on this campaign and the experiment results refer to Ramon Villarino's PhD thesis dissertation and Villarino et al. (2003).

2.2.2 The Plata Campaign

Scientists from Argentina, Brazil, Uruguay and US working within the framework of the South Atlantic Climate Change Consortium (SACC), sponsored by the Inter-American Institute for Global Change Research (IAI), have outlined a

2 Campaigns

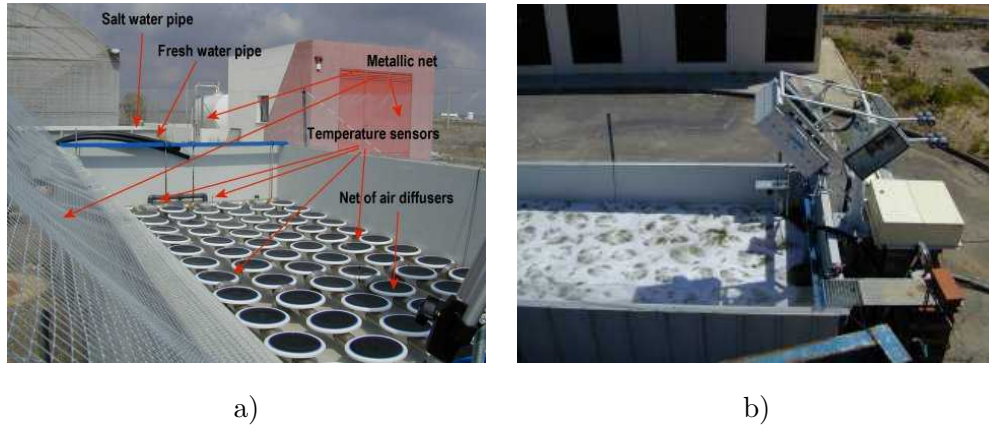


Figure 2.13: a) Visual description of the FROG experiment set-up, b) Radiometer pointing to the foaming pool.

research project to study the impact and variability of La Plata river (Argentina) plume on the adjacent ocean. The main goal of this project, co-financed by IAI and the U.S. Office of Naval Research, is to characterise the seasonal variations of the Plata plume and the Subtropical Shelf Front, their impact on the circulation and on the chemical and biological processes of the continental shelf.

With a mean annual discharge of $23590 \text{ m}^3/\text{s}$ of freshwater La Plata river produces an extraordinary impact over the continental shelf of northern Argentina, Uruguay and southern Brazil. The river waters are a significant source of nutrients, dissolved and suspended matter and, due to their low salinity, induce strong vertical stratification over the adjacent shelf. Studies based on historical hydrographic data (Piola et al., 2000) reveal that La Plata derived low salinity waters present seasonal fluctuations of several hundred kilometres over the shelf. Consequently, large seasonal variations of environmental conditions occur over the continental shelf of eastern South America between 38 and 25° S .

The first field activity carried out within the Plata project was a large-scale winter oceanographic survey and an airborne salinity measuring survey. The Plata winter survey was carried out between Mar del Plata, Argentina and Itajaí, Brazil, from 20 August to 2 September 2003.

The campaign was carried out on board the oceanographic vessel ARA PUERTO DESEADO. The vessel departed Mar del Plata, Argentina, 20 August 2003 at 12.15 local time and docked in Itajaí (Brazil) at 08.45 local time (GMT+3) 2 September 2003. 83 CTD stations were performed in eleven cross-shelf sections spanning from the near coastal region (10 nautical miles from shore) to the western boundary currents offshore, at depths greater than 1000 m (Figure 2.14a).

2.2 Other campaigns

The sections were designed to cover the area of influence of the Río de la Plata and the Patos/Mirim Lagoons over the shelf and its northward extension, characteristic of Austral winter. During the CTD stations salinity measurements were performed. Moreover the ship carried a thermosalinograph instrument, which measured sea surface salinity during the whole path of the ship.

The airborne survey was one of the components planned for the Plata project, funded by the ONRIFO (U.S. Office of Naval Research International Field Office), through the Naval International Cooperative Opportunities in Science and Technology Program, the IAI (Inter-American Institute for Global Change Research) and Uruguayan local funding. The survey was carried out on a CASA 212 Aviocar of the Fuerza Aérea Uruguaya (C-212 FAU 532). The mission consisted in a series of flights covering the study area, using the STARRS (Salinity, Temperature, and Roughness Remote Scanner) instrument, provided by the US Naval Research Laboratory.

Two kinds of surveys were planned (see figure 2.14a and b):

- Large surveys, intended to cover the positions of the oceanographic stations covered by the ARA PUERTO DESEADO. Flight altitude was normally 900 - 1200 m. The corresponding transects were named LEG1, LEG2 and LEG3.
- Small surveys, two located in the Río de la Plata (Plata Mouth and Plata Front), and a third at the mouth of the Patos Lagoon in Brazil (Patos Outflow). These flights were made at 2440 m. The data obtained allows the construction of a salinity map, with less space between consecutive track lines.

The STARRS instrument has 6 antennas and measures only at V-pol, as explained before. In this case the instrument was not tilt, so the measurements were performed at the incidence angles of -38.5° , -21.0° , -6.5° , 7.5° , 22.0° and 38.5° .

The surveys were made at night, in order to avoid the interference from sun glint. There were in total more than 45 hours of survey, and more than 7200 nautical miles of navigation.

Sea surface salinity is an excellent indicator of the horizontal extent of riverine constituents over the continental shelf. Figure 2.14c presents the first truly synoptic sea surface salinity distribution constructed combining the Plata winter cruise CTD and thermosalinograph data after preliminary calibration. Because there are no waters fresher than 33.5 on the northern Patagonia continental shelf (Guerrero and Piola (1977)), all water fresher than 33.5 must contain La Plata mixtures. Thus, the 33.5 isohaline marks the outer edge of La Plata plume. Surface salinity shows a well developed, continuous near coastal plume extending

2 Campaigns

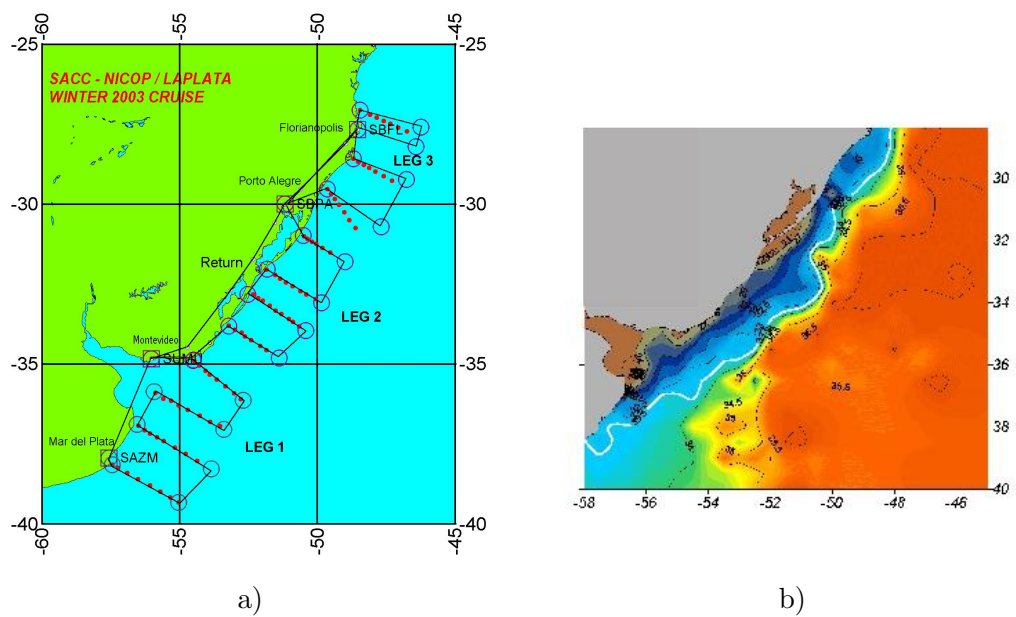


Figure 2.14: a) Ship CTD stations and the plane track overplotted in blue line. b) Sea surface salinity distribution as observed during the Plata winter cruise 2003. The white contour is the 33.5 isohaline, which marks the outer edge of La Plata plume. (from survey reports and Piola et al. (2000)).

2.2 Other campaigns

from La Plata estuary to 26° S, beyond the northernmost locations occupied during the cruise.

Another survey was performed in the same area under the same project, in February 2004, but calibrated data was not still available to be included in the analysis performed in this thesis.

More information on this campaign can be found in:
<http://glaucus.fcien.edu.uy/pcmya/sacc/LaPlataW2003/index.html>.

Acknowledgements: The L-band data from the Salinity, Temperature, and Roughness Remote Scanner (STARRS) was available thanks to the support of Office of Naval Research Global's NICOP program and the Naval Research Laboratory's Salinity Driven Advection in Littoral Deep Areas (SALIDA) project (award number NRL BE-435-017) and its participants. The ship-based in-situ temperature and salinity data were graciously provided by Argentina's Servicio Hidrografia Naval as part of the multi-national (Argentina, Brazil, Uruguay, and USA) "La Plata" campaign which was conducted under the auspices of the South Atlantic Climate Change consortium sponsored by the Inter-American Institute for Global Change Research (IAI).

2 Campaigns

Chapter 3

Modelling the brightness temperature of the sea

This chapter presents a review on the most accepted models existent in the literature that describe the natural emissivity of the sea at L-band. Some of the models presented here are based on theoretical approaches and others are semi-empirical propositions. Also a new semi-empirical model, developed by the author, is presented. This new model, based on WISE dataset, is analysed and compared with other models. In chapter 5 some of these models will be used to retrieve salinity from campaign measurements, and depending on the quality of the retrieved salinity the models will be evaluated.

3.1 Theoretical models

One of the main tasks for the SMOS science development team is to select the forward models that best describe the natural sea surface emissivity process. This is a key issue since the SSS retrieval algorithm for SMOS will be based on these models.

To perform this work in situ measurements are needed, to enable to choose the model that best fits measured data. However, at L-band very few campaigns have been performed, and very few data sets were acquired. For this reason, ESA sponsored the three campaigns, WISE, EuroSTARRS and LOSAC (Wursteisen, P. and Fletcher, P. (2003)), which permitted to acquire a wealth of in situ data, and allow scientists to advance significantly. However, it is not still clear now what will be the best model to use in the retrieval algorithm, and more data is needed. ESA is planning to perform a large airborne campaign in 2005, called CoSMOS to address several of the open issues.

As presented earlier, sea emissivity is governed by some geophysical parameters, as salinity, temperature, sea surface roughness, foam (if present). Emissivity also depends on the sensor parameters: frequency, incidence angle (θ), azimuth look direction (ϕ), and polarisation (p).

To express sea surface emission at L-band, three different kind of models are necessary:

- **Dielectric constant model**, which from surface salinity, sea surface temperature and frequency data, allows to predict the complex dielectric constant value.
- **Sea roughness spectrum**, which describes the spectrum of sea surface when roughness is present (not flat surface). A good knowledge of this model is important since a different modulation of sea roughness spectrum will lead to different values of emission.
- **Electromagnetic scattering model**, which describes the way in which energy is scattered from sea surface when roughness is present.

3.1.1 Dielectric constant models

In section 1.3.1 the dielectric constant, ε , has been presented, and it has been explained that it depends on frequency, temperature and salinity.

Several models of sea water complex permittivity exist in the literature. However, most of them have been obtained for frequencies higher than L-band.

Also several expressions have been obtained from measurements performed with NaCl solutions, but an important difference in the permittivity obtained

using purely NaCl waters with respect to sea waters has been reported (Ellison et al., 1998).

At L-band the most accepted models are the ones proposed by Klein and Swift, Ellison et al., and more recently by Blanch and Aguiasca.

All the authors base the permittivity model on the Debye expression (equation 1.11), and using different techniques they obtain experimental values for the following variables: ϵ_s static dielectric constant, τ relaxation time, σ ionic conductivity. These variables are a function of salinity and temperature.

Klein and Swift dielectric constant model

During the 70's Ho and Hall (1973) and Ho et al. (1974) performed measurements of the dielectric permittivity at L- and S-band with NaCl solutions and sea water samples. The precisions on the measurements at L-band were of 0.2% and 0.4% for the real and imaginary part, respectively.

Later on, in 1977 Klein and Swift (1977) did a reanalysis of the same measurements, and they found a bias on the ϵ_i measured by Ho et al. Thereby, they proposed a new ϵ_i formulation, which appeared to have more precision.

The accuracy of the model they proposed is at least of 0.3 K in the brightness temperature, and it should be valid for salinities in the range from 4 to 35 psu.

However, there were very few measurements done on the salinity range from 30-40 psu, which are the most common values in the world's oceans.

Ellison et al. dielectric constant model

Ellison et al. (1998) measured the complex permittivity at the laboratory for several frequencies between 6-90 GHz. The technique chosen at low frequencies was to measure the transmission coefficient with a coaxial line method.

The water samples were collected at sea, and covered most of the physical conditions found in the world's oceans.

To model the permittivity of sea-water at 1.43 GHz, the authors extrapolated the results from higher frequencies. This could be one of the reasons why this model is a little bit divergent from the other two models.

Blanch and Aguiasca dielectric constant model

In Blanch and Aguiasca (2004) a new method for computing the permittivity of sea water has been used. They proposed a static structure based on the propagation method, using a standard rectangular waveguide, which has two transitions for the input signal and one for the output signal that will be measured.

3 Modelling the brightness temperature of the sea

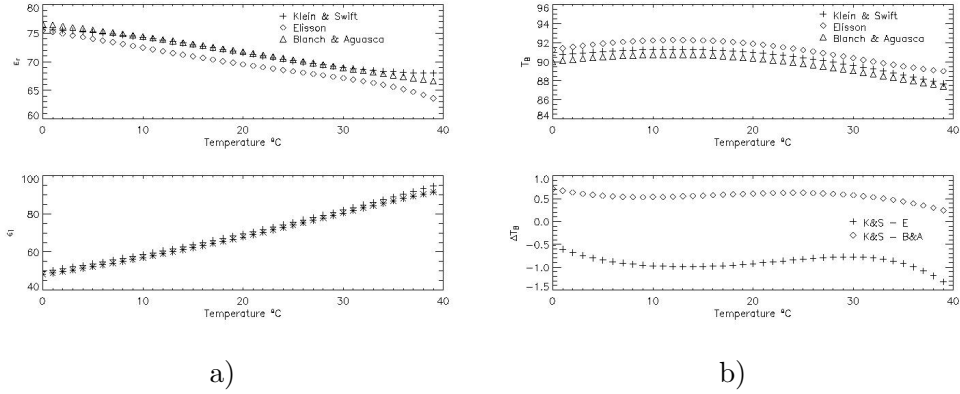


Figure 3.1: Comparison of three different permittivity models. a) Real and imaginary parts of permittivity at 1.4 GHz, for salinity of 37.5 psu, b) Brightness temperature for normal incidence, for salinity of 37.5 psu at 1.4 GHz.

The measurements were done at 1.43 GHz, with seawater samples with salinities in the range of 0-40 psu, in steps of 2 psu for low salinities, and steps of 1 psu for high salinities. The temperature changed from 0° to 40°, in steps of 0.7°. The authors curve-fitted the equations with the results, and they finally got their model.

Figure 3.1 shows a comparison of the three models presented above. It shows that Klein & Swift and Blanch & Aguiasco, are quite similar for mid temperatures, while Ellison model differs a bit from the others, specially for the real part of the permittivity. Also, the K&S and B&A models give similar results on brightness temperature, while Ellison tends to overestimate it.

Recently, William Wilson from JPL performed L-band radiometric brightness temperature measurements in a saltwater pond as a function of salinity and temperature. They conclude in Wilson et al. (2004) that measurements are in good agreement with the Klein and Swift dielectric model over a temperature range from 8° to 32° C and a salinity range from 25 to 40 psu.

3.1.2 Wave spectrum theoretical models

Sea surface spectrum models are the basic statistical tools used for the rough sea surface description within asymptotic emissivity models and their range of validity are therefore very important for SSS retrieval algorithms accuracy.

Durden & Vesecky

Durden and Vesecky (1985) empirical sea surface spectrum model was one of the first used for describing the electromagnetic scattering. This model is commonly used jointly with two-scale and SPM/SSA models for the emissivity scattering modelling. Surprisingly this wave spectrum model multiplied by two provides improved results when used in asymptotic models for computing sea surface emissivity. This model is only applicable for fully developed seas, i.e. seas that are in equilibrium with the local winds. Thereby this wave spectrum is described uniquely with the wind vector at 1.4 GHz.

Elfouhaily

Elfouhaily et al. (1997) developed the so-called 'unified spectrum', solely from in situ measurements. The main characteristic of this model is that it is dependent on the age of the waves, by the parameter u^*/C_p for which u^* is the surface wind friction velocity and C_p is the phase speed of the waves at the peak of the spectrum. This model reproduces the significant wave-height for developing seas.

Kudryatsev

Kudryatsev et al. (1999) presented a new model where a new physical approach of the short wind wave spectrum is used, which takes into account the statistical properties of breaking waves and the mechanisms of capillaries generation. Here, analytical expressions for the spectral forms are deduced from the theoretical energy sources equations. The age of the waves is taken into account here, also.

A restriction of some of these wave spectrum models is that they consider fully developed seas. The models that takes into account the wave age, theoretically can deal with partial developed seas, but in practise it is very difficult to evaluate this parameter. Miranda et al. (2003) emphasis that the fully developed sea condition are an unusual situation in real case, since usually the sea is growing

3 Modelling the brightness temperature of the sea

or decreasing. Also it should be underlined that these models do not consider the occasions where the sea state is not dependent on local wind, but on far and ancient winds, as happens when swell is present.

3.1.3 Surface roughness scattering models

The emissivity of a calm, smooth sea surface may be calculated by using the specular Fresnel reflection expression given in 1.9 and 1.10. However, when the surface is roughened by wind action, its emissivity and scattering behaviour become more complicated.

Two main asymptotic theories have been used as potential forward models for SMOS, and they are briefly described in the following.

Two-scale models

The Two Scale Method (TSM) approximates sea surface as a two-scale surface, with small ripples or capillary waves (small scale compared with electromagnetic waves) on the top of large-scale waves characterised by their distribution of slopes. Then, the thermal emission of sea surface is the sum of emissions from individual, slightly perturbed surface patches tilted by the underlying large-scale surface.

The geometric optics approximation is applied for long scale wavelengths, while Small Perturbation Method is used for short scale wavelengths. The problem, here, is that the division of the ocean surface into small and long scales remains an unclear process, and the parameter which divides the two scales is often arbitrarily chosen within wide limits. Different authors make different choices which range from $k_0/1.5$ to $k_0/40$ (being k_0 the electromagnetic wavenumber), and the optimal wavelength for the spectrum split has been found to be incident angle dependent.

At L-band, Dinnat (2003) has however shown that small changes in this parameter do not have a significant influence on the emissivity of the sea surface.

The maximum permitted value of wind speed for this model is 19 m/s, a very unusual value to reach. Consequently, there is no practical restriction in the use of this model for sea surface emissivity simulations.

The Two-scale model that has been used in this work is developed by Yueh et al. (1997), which fix the cut-off value to $k_0/3$ and use Durden & Vesecky wave spectrum multiplied by two.

Figure 3.2 compares the sensitivity of the brightness temperature to the wind speed with the two scale method for different spectra: Elfouhaily, Durden & Vesecky and Durden & Vesecky $\times 2$.

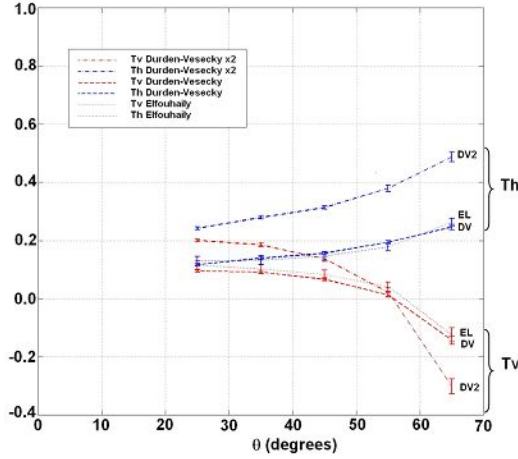


Figure 3.2: Comparison of the derivative of the brightness temperature with respect to wind speed, $\Delta T_{B\ rough}/\Delta U_{10}$, as function of the incidence angle, when Two Scale Method (Yueh et al., 1997) is used with Durden & Veseky, Durden & Veseky $\times 2$ and Elfouhaily wave spectrums (from Camps et al. (2003b)).

SSA/SPM model

Several authors have shown that expressions obtained from the SPM (Small Perturbation Method) for surface emissivity have the form of a small-slope, and not small height, expansion. Some comparisons have shown that SPM and SSA (Small Slope Approximation) are equivalent for the thermal radiation, and not for differential scattering coefficients. It has been found that errors in scattering cross-section in the near specular region are compensated by errors outside the specular region, so the integration still produces an accurate emission prediction. No artificial cut-off wavenumber is required to separate small from long waves and SSA can be applied to the entire ocean surface spectrum. Only the second order expansion is considered in this study.

The input values to the model are SSS, SST, wind speed, azimuth and incidence angle.

Figure 3.3 compares the sensitivity of the brightness temperature to the wind speed with SSA for different spectra: Elfouhaily, Kudryatsev and Durden & Veseky $\times 2$.

An exhaustive comparison of these scattering and wave spectrum models, plus others which have not been described here (Kirchhoff model, integral equation method...), is performed in Vall-llossera et al. (2003). This work reviews the

3 Modelling the brightness temperature of the sea

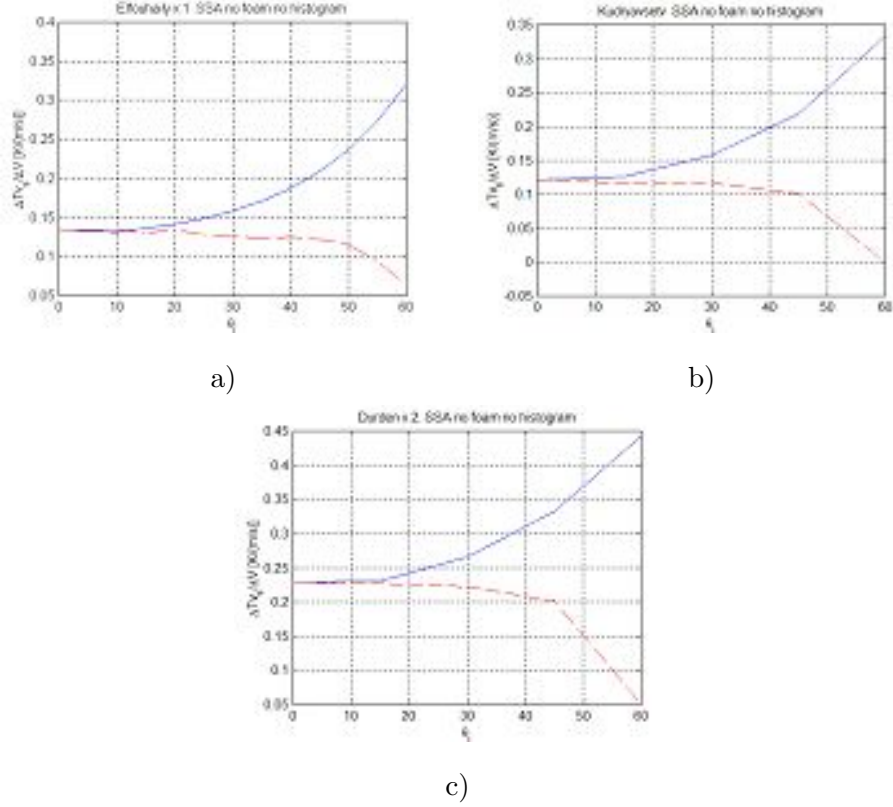


Figure 3.3: Comparison of the dependence of $\Delta T_H / \Delta U_{10}$ (continuous line) and $\Delta T_V / \Delta U_{10}$ (dashed line) respect to the incidence angle predicted by SSA model when different spectra are used: a) Elfouhaily spectrum, b) Kudryavsetv c) Durden & Veseky $\times 2$ (from Vall-llossera et al. (2003)).

difference on the dependences of T_B to wind speed between the models, and compares these results with WISE campaign measurements.

Furthermore reviews on these theoretical models have been preformed in the ESA studies ITT/1-4314/02/NL/AG, WP1200 and ITT 1-4505/03/NL/Cb WP1100.

3.2 Semi-empirical models for sea surface emissivity

The semi-empirical models of the emissivity of the sea surface are obtained from experimental data. In particular the models presented below have been derived from WISE 2000 and 2001 campaigns.

The brightness temperature of the sea surface can be modelled by 3.1, composed by a term due to the emissivity of a flat surface plus another term that accounts for the effect of the sea roughness,

$$T_{B,p}(\theta_i, SST, SSS, C_n) = T_{B\text{ Fresnel},p}(\theta_i, SST, SSS) + \Delta T_{B\text{ rough},p}(\theta_i, C_n, SST, SSS) \quad (3.1)$$

where,

$$\begin{aligned} T_{B\text{ Fresnel},p}(\theta_i, SST, SSS) &= SST \cdot e_p(\theta_i, SST, SSS) \\ &= SST \cdot (1 - |R_p(\theta_i, SST, SSS)|^2) \end{aligned} \quad (3.2)$$

and R_p are the Fresnel field reflection coefficients with p polarisation as defined in equation 1.10, which depends on the dielectric constant.

The second term of the equation 3.1 describes the emissivity due to the roughness of sea. This term is theoretically poorly known, and it is determined by the wave spectrum, which is also unsatisfactorily known. This term is dependent on incidence angle, C_n that represent the parameters used to describe the roughness of the sea (U_{10}, SWH, \dots), SSS and SST. The last two have not been considered in the regressions done from WISE data set since, they were very stable. However, Etcheto et al. (2004) have observed a small dependence of $\Delta T_{B\text{ rough},p}$ to SST with WISE and EuroSTARRS data-sets.

In this section some empirical models to describe the term $\Delta T_{B\text{ rough},p}$ are presented.

3.2.1 Wind speed dependence

Hollinger (1971) derived the brightness temperature sensitivity to wind speed from the measurements made at Argus Island Tower, and described it as follows:

$$\begin{aligned} \Delta T_h &\approx 0.2 \left(1 + \frac{\theta_i}{55^\circ}\right) U_{10} \\ \Delta T_v &\approx 0.2 \left(1 - \frac{\theta_i}{55^\circ}\right) U_{10} \end{aligned} \quad (3.3)$$

3 Modelling the brightness temperature of the sea

valid only for incidence angles (θ_i) smaller than 55° . This model was used by the National Oceanic and Atmospheric Administration (NOAA) for their experiments in 1997 with the SLFMR sensor (Goodberlet and Miller (1997)).

Camps et al. (2004a) have, also, calculated the brightness temperature sensitivity to wind speed based on WISE campaign data. A linear empirical model was obtained from fitting to the data $\Delta T_{B,rough}$, and it is defined as follows:

$$\begin{aligned}\Delta T_h &\approx 0.23 \left(1 + \frac{\theta_i}{70^\circ}\right) U_{10} \\ \Delta T_v &\approx 0.23 \left(1 - \frac{\theta_i}{50^\circ}\right) U_{10}\end{aligned}\tag{3.4}$$

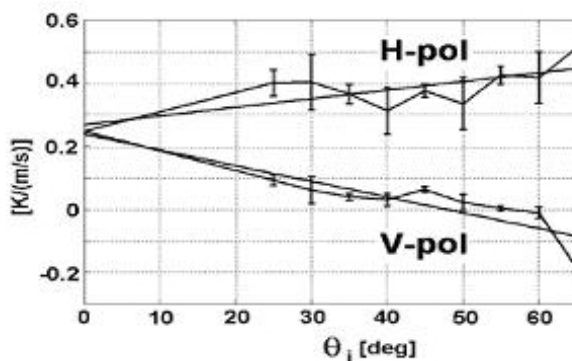


Figure 3.4: WISE 2001 derived L-band brightness temperature sensitivity to wind speed, for all data points.

The extrapolated sensitivity of T_B to wind speed is shown in figure 3.4, and at nadir is then,

$$\frac{\Delta T_{B,p}(\theta_i = 0^\circ)}{\Delta U_{10}} \approx 0.23 \text{ K}/(m/s)\tag{3.5}$$

The correlation between the data points and the linear fit is quite high, for H-pol, $r_h = 0.74$ and for V-pol, $r_v = 0.89$.

Since most of the data measured in the campaign were obtained under low wind conditions (45% of the measurements recorded with U_{10} in the range 0-5 m/s), it is evident that an error in the computed sensitivity at low winds has a very large impact in the weighted average. So Camps et al. (2004a) proposed also a new model that considers only data points that correspond to wind speed at 10 m high larger than 2m/s (below that, strange behaviours have been observed), with atmospheric instabilities corrected. Equations are written here:

3.2 Semi-empirical models for sea surface emissivity

$$\begin{aligned}\Delta T_h &\approx 0.25 \left(1 + \frac{\theta_i}{188^\circ}\right) U_{10} \\ \Delta T_v &\approx 0.25 \left(1 - \frac{\theta_i}{45^\circ}\right) U_{10} \quad U_{10} \geq 2m/s\end{aligned}\tag{3.6}$$

The correlation coefficients between data points and the linear regression lines are: $r_h = 0.79$ and $r_v = 0.90$, which are higher than before.

3.2.2 Wave height dependence

In the same paper Camps et al. have studied the brightness temperature sensitivity to significant wave height¹ (*SWH*). Here it is considered that $\Delta T_{B\,rough,p}$ is expressed only through the *SWH* in meters. The linear fit of the measurements brings to the following model:

$$\begin{aligned}\Delta T_h &\approx 1.09 \left(1 + \frac{\theta_i}{142^\circ}\right) SWH \\ \Delta T_v &\approx 0.92 \left(1 - \frac{\theta_i}{51^\circ}\right) SWH\end{aligned}\tag{3.7}$$

With correlation coefficient of $r_h = 0.88$ and $r_v = 0.78$, and the extrapolated sensitivity at nadir is then,

$$\frac{\Delta T_{B,p}(\theta_i = 0^\circ)}{\Delta SWH} \approx 1 \text{ K/m}\tag{3.8}$$

3.2.3 Wind speed and wave height dependence

Until the moment, most of the models (theoretical or semi-empirical) describe the brightness due to roughness of the sea as a function of wind speed only. Therefore, these models assume that the roughness of the sea is only dependent on the local wind speed. This is not completely right, since, when swell is present, some events of low local wind speed and high wave height are possible. Figure 3.5 shows the relationship between wind speed and significant wave height measured at the same time by the same buoy during WISE2001. It shows that the correlation is high between both parameters, but there are some events where high *SWH* were observed and U_{10} was low.

Miranda et al. (2003) showed, also, that the measured spectra frequently are not well approximated using fully developed models, since commonly situations with growing and decaying winds have been recorded.

¹SWH is defined here as the average of the highest third of the waves.

3 Modelling the brightness temperature of the sea

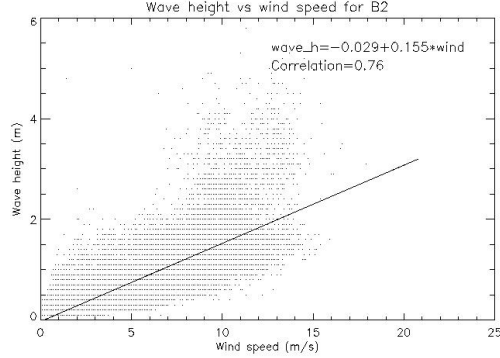


Figure 3.5: Scatter plot of SWH vs U_{10} with the liner regression line and the correlation with the data.

Being aware of this limitation, the author decided to try to find a model that takes into account also the swell events. That is to encounter a new model dependent on the local wind speed, as well as on the significant wave height. The derivation of this model, as well as test and comparison with other models, is a direct contribution of the author and it represents an important part of this thesis. This work has been published in Gabarró et al. (2004a) and has been presented in several conferences and meetings.

WISE 2001 data set was used to derive this new model. For each measurement of the radiometer, the wind speed and the wave height were obtained from the Aanderaa CMB buoy. Using 270 measurements, the curve fit IDL function was used to find the parameters that best fit the in situ measurements to the following model equation:

$$\begin{aligned}\Delta T_h &= (A + B \theta_i) U_{10} + (C + D \theta_i) SWH \\ \Delta T_v &= (A + E \theta_i) U_{10} + (C + F \theta_i) SWH\end{aligned}\tag{3.9}$$

The results obtained with their standard deviation are written in the following table:

3.2 Semi-empirical models for sea surface emissivity

| | Result | Standard deviation |
|---|--------|--------------------|
| A | 0.119 | 0.063 |
| B | 0.005 | 0.001 |
| C | 0.593 | 0.375 |
| D | -0.012 | 0.008 |
| E | 0.003 | 0.001 |
| F | -0.012 | 0.008 |

Finally the model derived from WISE data can be written as follows:

$$\begin{aligned}\Delta T_h &\approx 0.12 \left(1 + \frac{\theta_i}{24^\circ}\right) U_{10} + 0.59 \left(1 - \frac{\theta_i}{50^\circ}\right) SWH \\ \Delta T_v &\approx 0.12 \left(1 - \frac{\theta_i}{40^\circ}\right) U_{10} + 0.59 \left(1 - \frac{\theta_i}{50^\circ}\right) SWH\end{aligned}\quad (3.10)$$

The correlation coefficient between the data points and the model is $R = 0.761$. It should be stressed that comparing equation 3.10 with 3.6 and 3.7 at nadir, for this model, the dependence on U_{10} is almost half of the value given by the wind speed model, and that the dependence on SWH is close to the half of the sensitivity given by the model dependent on SWH .

The goodness of fit of the regression, called the *regression of determination*, is $r^2 = 60.1\%$. The absolute magnitude of the goodness of fit is the standard error of the estimate, that is defined as follows:

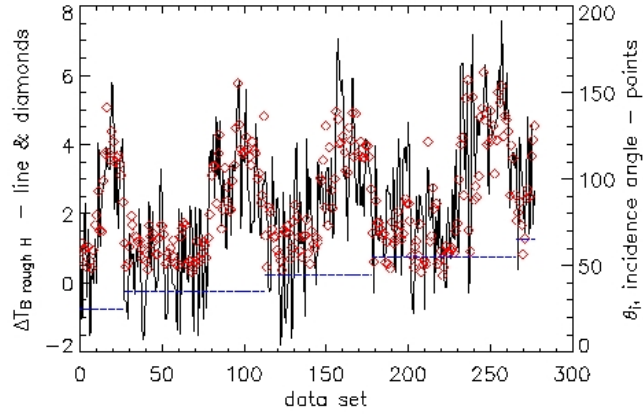
$$\text{Standard error of the estimate} = \left[\frac{1}{N_{data} - n_{param}} \sum_{i=1}^N (y - \hat{y})^2 \right]^{1/2} = 1.275K \quad (3.11)$$

where N_{data} is the number of data to fit the curve, and n_{param} is the number of parameters to estimate (Emery and Thomson (1997)).

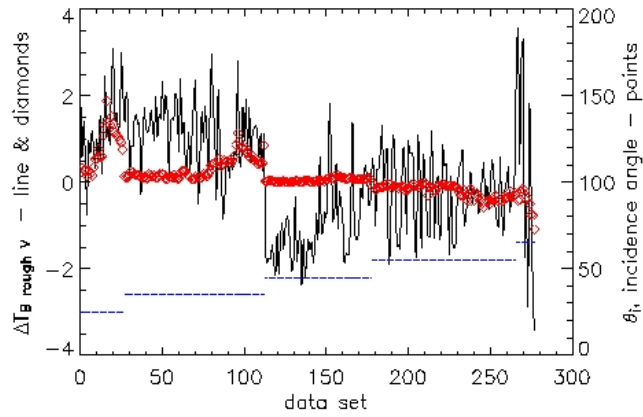
Figure 3.6 compares the $\Delta T_{B\text{rough}}$ measured and computed with this model for the two polarisations. The correlation at H-pol between them is 0.723, and the correlation at V-pol is 0.423, considerably lower as shown in the plot. The incidence angle of each measurement is also plotted, and it is represented through the right axis. Plot b) indicates that at incidence angles between 35 and 55 the $\Delta T_{B\text{rough}}$, V-pol of the model is near to zero, since the sensitivity of this to U_{10} and SWH is close to zero (the empirical model dependent on U_{10} only presents a similar behaviour). Then the high variability observed in the measurements should be due to experimental noise.

From here to the end, this new model will be called model-2P, as it is dependent on two parameters.

3 Modelling the brightness temperature of the sea



a)



b)

Figure 3.6: a) On left axis, the black line is $\Delta T_{B \text{ rough}}$ measured by the radiometer and the red diamonds are $\Delta T_{B \text{ rough}}$ obtained from the model presented in equation 3.10 at H polarisation for 270 data points. Incidence angles values (25° , 35° , 45° , 55° , 65°) are plotted with blue dots, referred at the right axis. b) The same for V polarisation.

3.3 Conclusions

Three different dielectric constant models have been presented and compared.

Also several direct models of the emissivity of sea surface at L-band have been presented. First the theoretical models have been shortly described. Later, two semi-empirical models derived by the UPC team have been presented.

Finally a new semi-empirical model, formulated by the author, that express the brightness temperature due to the roughness of the sea, is presented. The new approach in it is that sea roughness is expressed through both wind speed and significant wave height.

The advantage of this last model with respect to the others is that it considers the cases where swell is present (which is expressed in the SWH parameter) and the cases where small capillary waves are present due to local wind (which is expressed in the U_{10} parameter).

In chapter 5, these models will be compared by calculating the salinity retrieval from campaign datasets, and an analysis of the quality of them will be given, based in real data.

An interesting future work would be to try to derive other semi-empirical models using other parameters, in the way to better adjust models to real emissivity. Some other parameters that could be useful are: wave spectrum, wave edge, wind friction, etc. In section 4.4 a list of potential auxiliary parameters, that could be needed for SMOS is presented.

In chapter 6 the models will be compared using images created by the SMOS simulator.

3 Modelling the brightness temperature of the sea

Chapter 4

Auxiliary Parameters

This chapter presents the problem of the sensitivity of T_B auxiliary parameters, other than SSS.

Several sources of U_{10} and SWH that are currently available are introduced. Of course other sources are available, but the author has chosen few ones that are considered to have good accuracies and are representative of the whole possible sources. Hence data has been obtained from atmospheric or oceanographic models and satellite measurements.

Probably when SMOS will fly (2007) all these sources will not be available, or will be improved. But for the type of analysis done in this chapter, these sources are good enough. Finally a list of possible auxiliary parameters that could be used for SMOS is attached.

In chapter 5 the retrieved salinity errors when using different combinations of these sources will be analysed based in campaigns datasets.

4.1 Sensitivity to auxiliary parameters

The radiometer measurements at L-band are not only sensitive to salinity, but also to sea surface temperature and roughness of the sea, as has already been noted in the previous chapters.

This affirmation brings to a clear conclusion: In order to retrieve salinity it is required to know the parameters, that influence the brightness temperature. These parameters are called *auxiliary parameters*¹.

The question is now: 'How do we obtain these auxiliary parameters for SMOS?'. As explained before, the sensitivity of T_B to salinity is of the same order of magnitude or smaller than its sensitivity to SST and roughness of the sea.

Errors on T_B due to an error on an auxiliary parameter have been calculated by comparing the values measured by the radiometer with those obtained by the forward emissivity model when errors on U_{10} , SWH and SST are introduced. Figure 4.1 shows the difference $T_{B\text{ measured}} - T_{B\text{ modelled}}$, for different errors on the auxiliary parameters as function on the incidence angles. The plots have been done using WISE data set, and the emissivity model 2-P. The semi-empirical model that fits the dependence of T_B on both wind speed and significant wave height is used. The plots reveal that the most critical parameter is U_{10} , as pointed out by Yueh et al. (2001), and especially for the horizontal polarisation. An error on U_{10} of 3 m/s produces an error on T_B of ≈ 1.5 K. Less significant are the SWH errors, but they are not negligible at low incidence angles for V-pol.

Therefore, one can deduce that there is a need to know the auxiliary parameters with good accuracy, and as simultaneously in time and space as possible to the SMOS measurements.

One possibility is to use observations made by other sensors embarked on satellites with similar orbit, but these measurements will hardly be simultaneous. Meteorological and oceanographic marine models could also be used, with the advantage of higher temporal resolution, and that they assimilate satellite data and other sources of information. Both cases will present inaccuracies on the measurements due to instrumental errors and sampling limitations.

The advantage of SST with respect to the parameters that describe the roughness is that sea temperature has much less temporal variability than U_{10} , and so the variability is lower.

¹Sometimes, erroneously, they are also called ancillary parameters. Ancillary parameters are those recorded by the satellite, other than radiometric, and sent to ground in the same telemetry message (e.g. platform altitude).

4.2 Roughness parameter

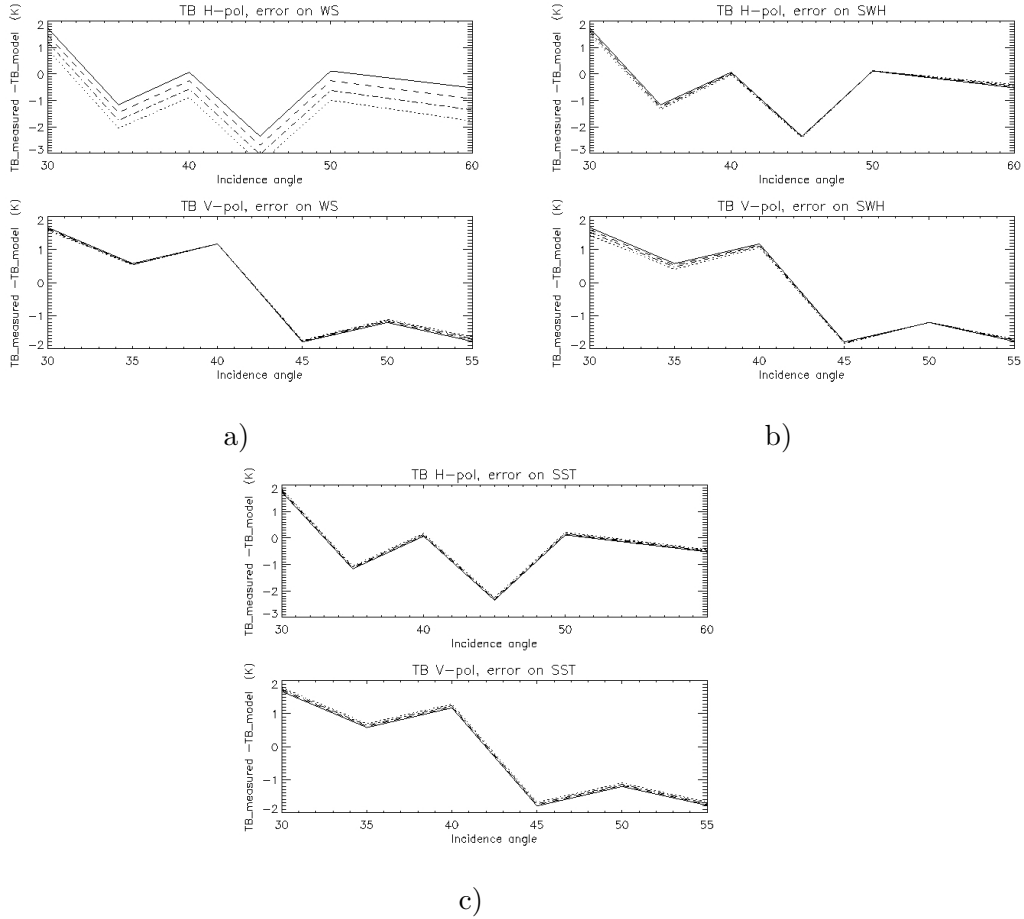


Figure 4.1: $T_{B\text{ measured}} - T_{B\text{ modelled}}$ as function of incidence angles, for H-pol (top) and V-pol (down). a) Case where errors on the U_{10} are added ($-\Delta U_{10}=0$, $--- \Delta U_{10}=1$, $- \cdot - \cdot \Delta U_{10}=2$, $\cdots \Delta U_{10}=3$ m/s). b) Case where errors on the SWH are considered ($-\Delta SWH=0$, $--- \Delta SWH=0.3$, $- \cdot - \cdot \Delta SWH=0.6$, $\cdots \Delta SWH=1$ m). c) Case where errors on the SST are added ($-\Delta SST=0$, $--- \Delta SST=0.3$, $- \cdot - \cdot \Delta SST=0.6$, $\cdots \Delta SST=1^\circ\text{C}$).

4.2 Roughness parameter

The determination of sea roughness coincidental to SMOS overpasses is a major problem due to its high variability and accuracy limitations in satellite measurements and models.

To analyse the effect on the SSS retrieval induced by different sources of roughness parameters, the following numerical model outputs and satellite measurements of wind speed and SWH were used for the area and time of WISE 2001 campaign:

1. Wind speed information:

- HIRLAM (High Resolution Limited Area Model): A numerical short-range weather forecasting system for operational use. This is the result of a big project of cooperation between several countries (Finland, Sweden, Norway, Denmark, The Netherlands, Ireland, Iceland and Spain, plus France as collaborator), to develop numerical prediction models for short range time. The analysis is done with wind and relative humidity as well as water temperature. It does assimilation of satellite data to give the best first guess to the numerical model. It gives predictions in temporal scales of 3 hours to some years. And the spatial scale goes from the global Earth to near 10 km. The products given by the model are: surface pressure, temperature, geopotential height, relative humidity and wind, all at surface and at several altitudes. It gives also accumulated precipitation every 6 hours.
- ARPÈGE (Action de Recherche Petite Echelle Grande Echelle): A numerical weather prediction system developed and supported by Météo-France and the European Centre for Medium range Weather Forecast (ECMWF) as part of the Aladin project. It is a numerical model with satellite assimilation. ARPEGE is a variable resolution spectral primitive equation system that runs with a semi-Lagrangian semi-implicit scheme.
- QuikSCAT: The SeaWinds instrument on the QuikSCAT satellite is a specialised microwave radar scatterometer that measures near-surface wind speed and direction under all weather and cloud conditions over Earth's oceans. NASA's Quick Scatterometer (QuikSCAT) was lofted into space on June 1999 into a polar orbit. SeaWinds uses a rotating dish antenna with two spot beams that sweep in a circular pattern. The antenna radiates microwave pulses at a frequency of 13.4 gigahertz across broad regions on Earth's surface. The instrument will collect data over ocean, land, and ice in a continuous, 1800 kilometer-wide

band, making approximately 400000 measurements and covering 90% of Earth's surface in one day.

2. Significant wave height information:

- WAM: WAM (CYCLE 4) is a third generation wave model, which computes spectra of random short-crested wind-generated waves. It is an energy balanced, spectral wave model with variable resolution. This version has incorporated improvements in the surface roughness and drag coefficients related to wave formation, as well as improved response to refraction effects from bottom topography. It defines the spectral energy of wind generated wave using 25 frequency bands and 24 direction bands. The finest resolution expected to be available, based on computer run time, input data and input wind field grid resolution is 5 minutes. The model performs best in water depths greater than 20 meters. The product generated is a gridded field that supplies wave height, period and direction for forecasts to 48 hours twice daily. WAM requires surface wind forcing from meteorological model output.
- RA-ERS: radar altimeter on board ESA ERS-2. The Radar Altimeter is a Ku-band (13.8 GHz) nadir-pointing active microwave sensor designed to measure the time return echoes from ocean and ice surfaces. Functioning in one of two operational modes (ocean or ice) the Radar Altimeter provides information on significant wave height; surface wind speed; sea surface elevation, which relates to ocean currents, the surface geoid and tides; and various parameters over sea ice and ice sheets. Significant Wave Height (H-1/3) is derived from the slope of the return echo leading edge, which is related to the standard deviation of the heights distribution of reflecting facets on the sea surface (assumed to be gaussian). ERS-2 was launched in 1995, and putted into a near-circular, polar, Sun-synchronous orbit, with a revisit time of 35 days.

The HIRLAM and WAM model outputs have been obtained through the Spanish Instituto Nacional de Meteorología and Puertos del Estado. The wind speed information from HIRLAM is analysed data, since assimilation of satellite and buoys data has been done to run the model. On the other hand, SWH data from WAM uses HIRLAM wind speed assimilated data but does not have assimilation of SWH data.

The ARPÈGE model belongs to Météo-France, and outputs have been obtained through LODYC. The data used here are analysed data, so assimilation from satellite or buoys measurements has been done.

4 Auxiliary Parameters

NASA's Quick Scatterometer Seawinds has a resolution of 25 kilometres and wind-speed measurements of 3 to 20 m/s have an accuracy of 2 m/s and an accuracy of 20 degrees on the direction measurements. It covers 90% of Earth's surface oceans in one day, but full repetition time is 3 days.

The SWH measured by the Radar Altimeter onboard ERS-2 for the Casablanca area during the WISE campaigns have been used. This instrument has an accuracy of 0.5 m or 10% whichever is higher, and a spatial resolution of $20 \times 20 \text{ km}^2$. The measurement is defined as 4 times the standard deviation of the wave slope (as buoy 3 in WISE 2001) in opposition to the definition of buoy 2 (average of the highest third of the waves). To convert from one definition to the other, the value according to the first definition must be divided by $\sqrt{2}$. The problem of the radar altimeter from ERS-2 is its low temporal resolution (35 days repetition), so to have data with the required time resolution, data from a huge area (170*440 Km) were used.

| SOURCE | Spatial resolution | Temporal resolution |
|----------|--------------------|---------------------|
| HIRLAM | 0.125° | 3 hours |
| ARPÈGE | 0.25° | 6 hours |
| QuikSCAT | 25 Km | 3 days |
| WAM | 0.125° | 3 hours |
| RA-ERS | 20 Km | 35 days |

Table 4.1: Comparison of different sources for wind speed and significant wave height.

Table 4.1 summarises the spatial and temporal resolutions of each data source. When accepting satellite data measured in an area (not only one point) the temporal resolution increases, since different satellite passes can be considered. Figures in 4.2 show the temporal sequence of wind speed and wave height obtained from these sources for WISE2001 time period; in situ measurements from buoys are also plotted. For wind speed, the models and satellite outputs are quite similar to in situ measurements except in some punctual occasions. The mean difference between wind speed in situ measurements and HIRLAM model output is 1.98 m/s, with respect to ARPÈGE model output is 1.93 m/s, while to satellite data is 1.59 m/s (although in this last case there are much less data points available). These differences are above the 1.5 m/s accuracy in wind speed initially required for SMOS SSS retrieval from preliminary simulations.

SWH's given by the model is similar to buoy measurements, except for high

4.2 Roughness parameter

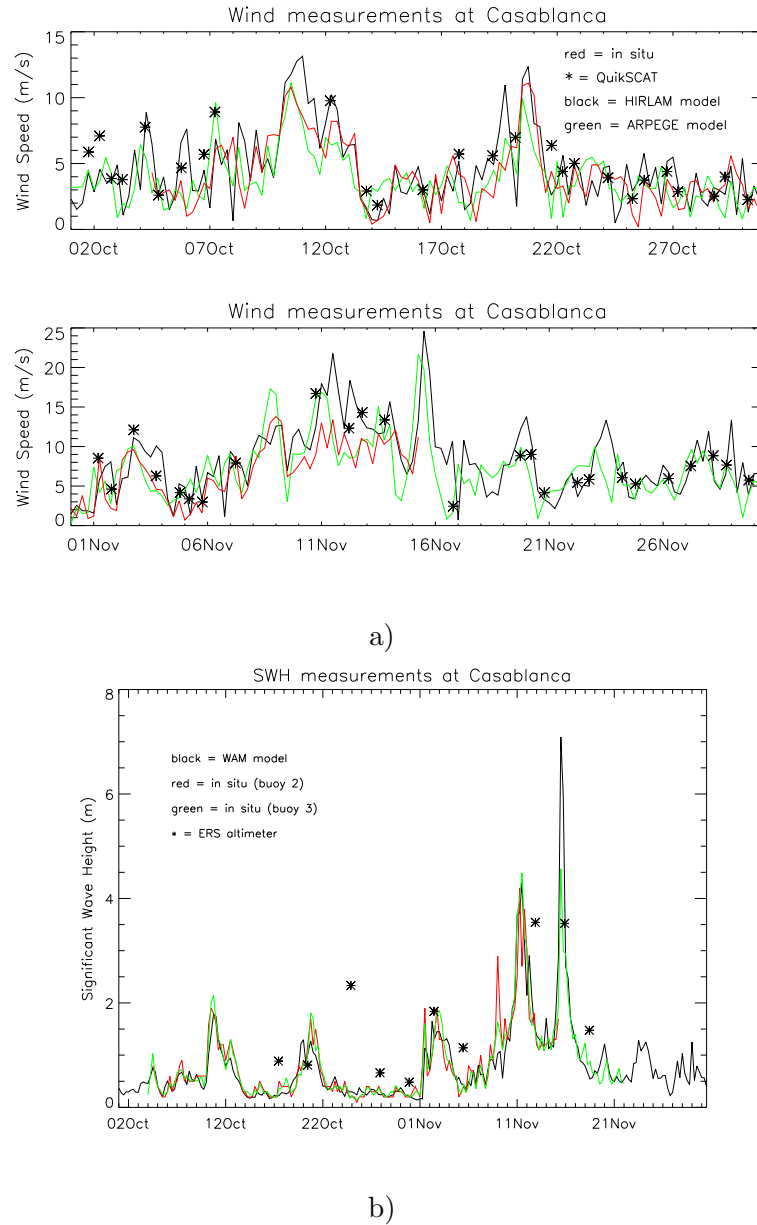


Figure 4.2: a) Comparison of different sources of wind speed information during WISE 2001 campaign. In situ buoy (red line), HIRLAM model (black line), ARPÈGE model (green line) and QuikSCAT satellite (*). b) Comparison of different sources of significant wave height information during WISE 2001 campaign. In situ data buoy 2 (red line), in situ buoy 3 (green line), WAM model (black line) and Radar Altimeter-ERS (*)

4 Auxiliary Parameters

wave height events, where the model overestimates them. The satellite measurements are not very realistic, which is not surprising since their temporal resolution is very low and a lot of spatial averaging has to be done to cover the WISE area. The mean difference between in situ measurements and WAM model is 0.22 m, while the mean difference grows to 1.16 m with respect to satellite measurements.

4.3 SST parameter

Sea surface temperature, nevertheless, is not as critical as roughness, since its variability is much lower, the sensitivity of T_B to SST is also lower, and satellite measurements are very accurate and frequent.

The brightness temperature sensitivities to SSS and SST, for all incidence angles and flat surface, and for salinities larger than 20 psu, are the following:

- $\Delta T_B / \Delta SSS \approx 0.35 - 0.80 K / psu$ at V-pol
- $\Delta T_B / \Delta SSS \approx 0.20 - 0.60 K / psu$ at H-pol
- $\Delta T_B / \Delta SST \approx 0.02 - 0.60 K / ^\circ C$ at V-pol
- $\Delta T_B / \Delta SST \approx 0.02 - 0.50 K / ^\circ C$ at H-pol

SST can be obtained with good accuracy and resolution by satellite measurements. A typical accuracy from Pathfinder data-set can be of approximately $\pm 0.3^\circ C$ in clear sky conditions and $\pm 0.5^\circ C$ otherwise. This error translates to T_B errors of 0.01- 0.3 K at V-pol and 0.01-0.25K at H-pol. So these errors on T_B are not significant, and will not represent a big problem for the salinity determination.

For this reason, this thesis has been focused on the roughness auxiliary parameters problems.

4.4 Other potential auxiliary parameters

A list of all the auxiliary parameters that can be potentially used in the retrieval of salinity by the SMOS mission is presented in table 4.2 and 4.3. This includes parameters that are strictly necessary (as SST) and others that will be used depending on the parameterisation finally selected to described the surface roughness impact on T_B . The table, that also includes the present accuracy and sources for these parameters, has been compiled within an ESA study (WP1100, ESTEC ITT 1-4050/03/NL/Cb) in which the author has been participated.

4.4 Other potential auxiliary parameters

| Parameter | Error | Source of auxiliary data | Usage |
|-----------------------------------|--|--|--|
| Sea surface temperature (SST) | $\pm 0.3^\circ\text{C}$ $\pm 0.5^\circ\text{C}$ | NOAA/AVHRR, ERS/ATRS, ENVISAT/AATSR MSG, Meteosat, GOES RMM/TMI, AMSR-E, models: ECMWF, NCEP | T_B direct model |
| Wind speed (U_{10}) | $\pm 2.5\text{ m/s}$ | ERS-2 AMI Wind scat., QuickSCAT, ADEOS-II, SeaWinds scatterometer, METOP-1 ASCAT, ENVISAT RA-2 Altimeter, JASON-1 Altimeter, DMSP's SSM/I radiometers, RadarSat, ENVISAT/ASAR, GPS models: ECMWF, NCEP | T_B direct model |
| Wind direction (ϕ_{10}) | $\pm 25^\circ$ | ERS-2 AMI Wind scat., QuickSCAT, ADEOS-II SeaWinds scatterometer, METOP-1 ASCAT, ENVISAT RA-2 Altimeter, JASON-1 Altimeter, DMSP's RadarSat, ENVISAT/ASAR, GPS, models: ECMWF, NCEP | T_B direct model |
| Air temperature (T_{air}) | $\pm 1^\circ\text{C}$ | models: ECMWF | Wind friction velocity, Foam coverage model |
| Fetch (F) | - | models: ECMWF (WAM) & NCEP (WAVEWATCH III) | T_B direct model |
| Wave aging parameter (Ω) | - | models: ECMWF (WAM) & NCEP (WAVEWATCH III) | T_B direct model |

Table 4.2: List of potential auxiliary parameters used to retrieve salinity for SMOS (from WP1100, ESTEC ITT 1-4505/03/NL/Cb).

4 Auxiliary Parameters

| | | | |
|--|----------------|---|-----------------------------|
| Significant wave height (H_s) | ± 0.25 m | models: ECMWF (WAM) & NCEP (WAVEWATCH III), ERS2 altimeter, TOPEX/POSEIDON, ENVISAT RA, JASON-1 Altimeter | T_B direct model |
| Peak Wave direction | ± 25 m | CMWF (WAM) & NCEP (WAVEWATCH III) ERS/AMI, ENVISAT/ASAR | T_B direct model |
| Peak wave period (T_p) | $\pm 20\%$ | ECMWF (WAM) & NCEP (WAVEWATCH III) | T_B direct model |
| σ_0 (dB) | - | GPS and radar | Direct roughness correction |
| Currents | < 0.5 m/s | detection by AVHRR, SeaWifs, SAR imagery, models: ORCA, CLIPPER, NANSEN | |
| Sea surface salinity (SSS) (first guess) | ± 0.25 psu | models: ORCA, CLIPPER, NLOM, in situ : ARGO floats, climatologies | T_B direct model |
| Oil slicks | detection | ERS-2, RadarSat, ENVISAT/ASAR | |

Table 4.3: Continuation of table 4.2.

Chapter 5

Salinity Retrieval

In this chapter the errors in the process of retrieving sea surface salinity from brightness temperature measurements of three campaigns are computed using different emissivity models and sources of auxiliary parameters.

The retrieved salinity errors are compared, and the discussion leads to choose a particular emissivity model, which better retrieves salinity.

Also the errors when using different sources of auxiliary parameters are presented. Since the retrieved salinity errors due to inaccuracies on the auxiliary parameters can be important, the author proposes a new method to obtain these parameters from the brightness temperatures themselves. This new method has demonstrated to retrieve salinity much better than fixing the parameters to erroneous values. However, this new method needs some adjustments and tuning.